Atmospheric Research 249 (2021) 105301

Contents lists available at ScienceDirect

Atmospheric Research

journal homepage: www.elsevier.com/locate/atmosres

The tornadoes of 30–31 May 2019 in south-Central Chile: Sensitivity to topography and SST

Julio C. Marín[a,b,*], Bradford S. Barrett[c], Diana Pozo[a,b]

[a] Department of Meteorology, Universidad de Valparaíso, Chile
[b] Centro de Estudios Atmosféricos y Astroestadística, Universidad de Valparaíso, Chile
[c] Oceanography Department, U.S. Naval Academy, Annapolis MD 21402, USA

ARTICLE INFO

Keywords:
Chile
Tornadoes
Mesoscale modeling
Topography
Sea-surface temperatures

ABSTRACT

Tornadoes were reported in south-central Chile on 30 and 31 May 2019. To better understand the mechanisms that supported the organization and severity of the storms that generated them, a series of high-resolution sensitivity simulations were conducted using the Weather Research and Forecast (WRF) model. In addition to a control simulation, three simulations were run that successively reduced the topography to 50%, 25%, and 0% of original height; three more simulations were run that increased SST by 2 K everywhere, decreased it by 2 K everywhere, and set all SSTs greater than 16 °C to exactly 16 °C; finally, two more simulations were run to explore the combined effects of SST changes and lower topography.

Results indicate that as topography was lowered, a strong northerly low-level jet along the upslope of the Andes weakened and broadened in both vertical and horizontal extent. Values of 0–6-km bulk shear and 0–3-km storm-relative helicity (SRH) over the regions where the tornadoes occurred diminished with successive reduction of the topography. As a result, simulated brightness temperatures were warmer, and swaths of updraft helicity were fewer and shorter. These results indicate that on 30–31 May 2019, flow blocking by the Andes topography generated mesoscale wind shear conditions that favored tornadoes. When SSTs were increased, instability (quantified by convective available potential energy, CAPE) also increased, although primarily offshore, and updraft helicity swath length increased, indicating a positive impact on simulated storm intensity. When SSTs were decreased, CAPE also decreased along with a decline in magnitude of updraft helicity. These results suggest that SSTs also impact storm severity via an influence on atmospheric instability. When the two factors were combined, warmer SSTs were not able to overcome a reduction in wind shear associated with a decrease in the topography. This suggests that in south-central Chile, wind shear is more important than CAPE for tornadic thunderstorms, as has been found for other regions around the world).

1. Introduction

Tornadoes are a form of extreme weather and have been studied for decades by researchers around the world (Brooks et al. 2019). The mesoscale conditions known to favor tornado formation from moist convection include thermodynamic instability, often quantified as convective available potential energy (CAPE; Davies-Jones 1986), and vertical wind shear, often quantified by deep-layer (0–6 km) and surface (0–1 km) bulk wind difference (Doswell III et al., 1996) and storm-relative helicity (SRH; Davies-Jones et al. 1990) in the 0–3-km and 0–1-km layers (Rasmussen and Blanchard 1998; Rasmussen 2003; Brooks et al. 2003; Potvin et al. 2010; Barrett and Gensini, 2013). Because many tornado studies focus on tornadoes in environments of both high CAPE and strong vertical wind shear, motivated in part because those environments tend to support most violent tornadoes (Thompson et al. 2003; Thompson et al. 2004; Cohen 2010), there remains a need to examine tornado occurrence in so-called "high-shear, low-CAPE" environments (Monteverdi and Quadros 1994; Hanstrum et al. 1998; Sherburn and Parker 2014; Barrett et al., 2020, hereafter B20). This is particularly important in regions where tornadoes are relatively rare events (Brooks et al. 2003) and where surface topography is complex (Blier and Batten 1994), which is the case for south-central Chile (35°–40°S).

At least two damaging tornadoes occurred in south-central Chile in May 2019 in this "low CAPE-high shear" environment less than 150 km upstream of the peaks of the southern Andes Mountains (3000 m at 35°S diminishing to 1000 m at 40°S). The Chilean National Weather Service (DMC, following its acronym in Spanish) conducted a formal analysis of

* Corresponding author at: Department of Meteorology, Universidad de Valparaiso, Valparaiso, Chile.
E-mail address: julio.marin@meteo.uv.cl (J.C. Marín).

https://doi.org/10.1016/j.atmosres.2020.105301
Received 12 May 2020; Received in revised form 17 September 2020; Accepted 1 October 2020
Available online 04 October 2020
0169-8095/ © 2020 Published by Elsevier B.V.

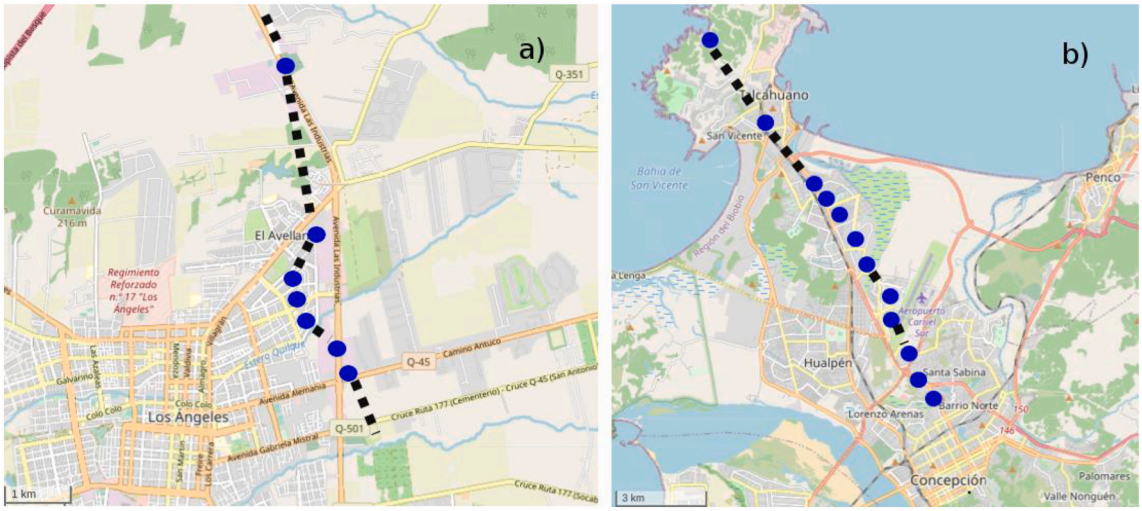

Fig. 1. Zoomed-in maps showing the paths (dashed black lines) of (a) the tornado that affected the city of Los Angeles on 30 May 2019, and (b) the tornado that affected the cities of Talcahuano and Concepción on 31 May 2019. The blue circles represent zones where damage was reported (based on V19).

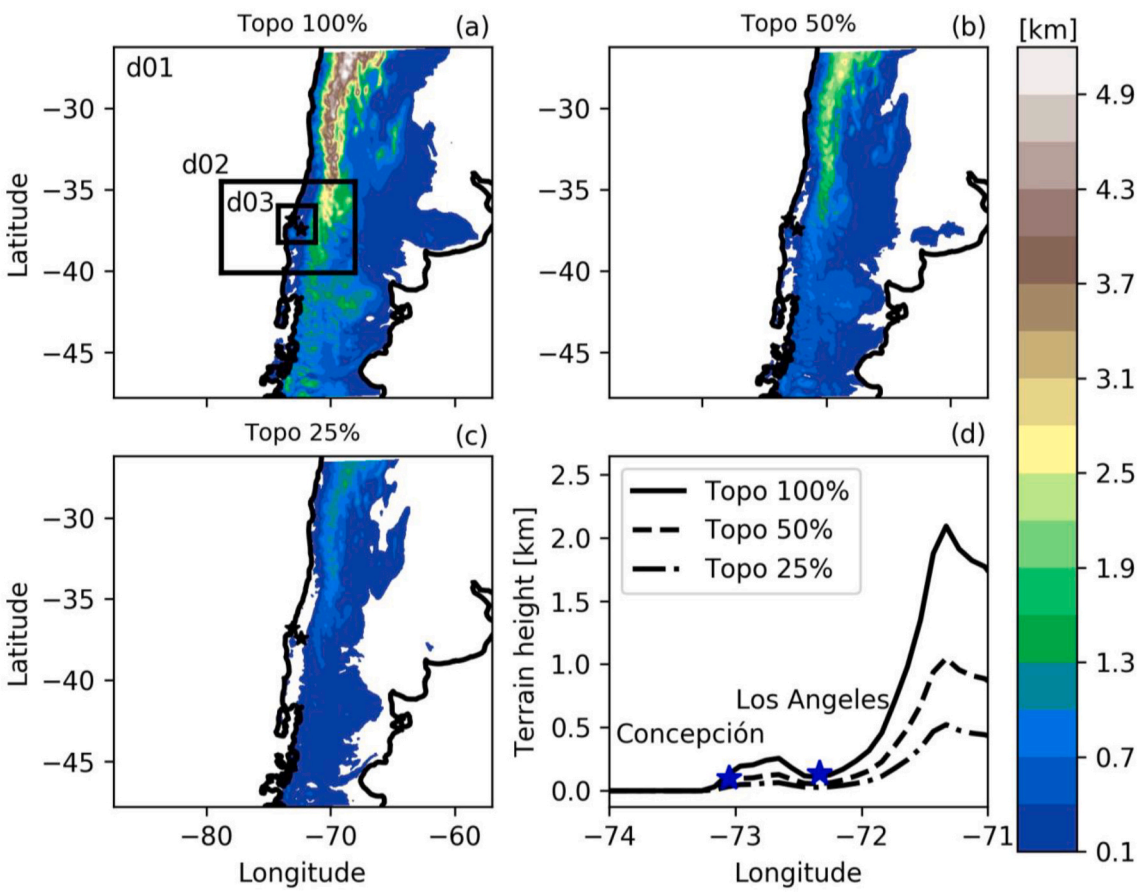

Fig. 2. Terrain height (color shaded) in domain one from (a) the CTRL, (b) Sim_50p, and (c) Sim_25p simulations. (d) Vertical cross-section of terrain height from domain 1 at the latitude of the city of Concepción (36.8333°S), for the CTRL, Sim_50p, and Sim_25p simulations. Additionally, the domain setting used in each numerical experiment is drawn in (a). Blue stars show the locations of the cities of Los Angeles and Concepción.

the damage and synoptic features associated with these events (Vicencio et al. 2019; hereafter V19), and B20 analyzed the atmospheric conditions that supported the formation of these tornadoes from the synoptic, mesoscale, and intraseasonal perspectives. As a result of the analyses of V19 and B20, several key questions emerged, particularly around the role of the Andes topography and observed SST anomalies and whether those features contributed to create conditions favorable for severe thunderstorms and tornado formation. This present study is motivated to answer those questions and better understand the connections between the atmospheric parameters and the physical environment that led to the tornadoes in this unique geographical zone.

The Andes cordillera is a major geographical feature of all of Chile. Its topography significantly modifies the climate regimes of the entire South American continent (Garreaud 2009). One such modification

Table 1
Simulations performed in this study and their differences with the CTRL simulation.

Name	Differences with CTRL simulation
CTRL	–
Sim_50p	Topography reduced to 50% of the original topography in all domains.
Sim_25p	Topography reduced to 25% of the original topography in all domains.
Sim_0p	Topography reduced to 0% of the original topography in all domains.
SST-2 K	SST uniformly reduced by 2 °C over all domains.
SST + 2 K	SST uniformly increased by 2 °C over all domains.
SST16C	SST values greater than 16 °C were reduced to 16 °C in the northwest parts of all domains.
SST-2 K_0p	Both topography reduced to 0% of the original topography and SST uniformly reduced by 2 °C over all domains.
SST + 2 K_0p	Both topography reduced to 0% of the original topography and SST uniformly increased by 2 °C over all domains.

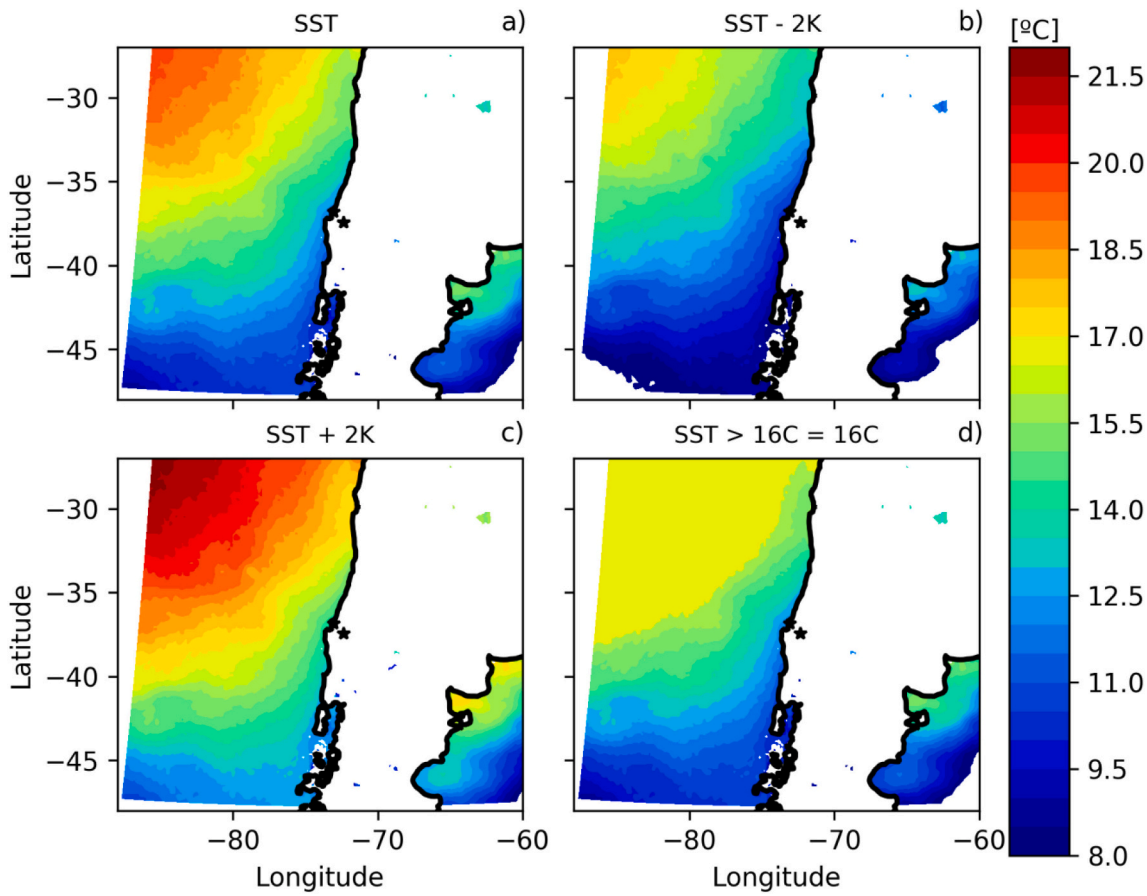

Fig. 3. SST distribution in domain one of the a) CTRL, b) SST-2 K (decreasing SST uniformly by 2 °C), c) SST + 2 K (increasing SST uniformly by 2 °C), and d) SST16C (eliminating the strong SST gradient to the NW of the domain) simulations. Black stars show the locations of the cities of Los Angeles and Concepción.

comes from flow blocking in the lower troposphere, which leads to the development of northerly barrier jets oriented parallel to the cordillera (Barrett et al. 2009; Viale and Norte 2009; Barrett et al. 2011; Viale et al., 2013), similar to the southerly barrier jets that develop windward the Sierra Nevada mountains (Parish 1982; Yu and Smull 2000) in response to an ageostrophic acceleration (Marwitz 1987; Overland and Bond 1993) in the direction of the barrier. Garreaud and Muñoz (2005) and Muñoz and Garreaud (2005) document the southerly (equatorward) low-level jet (LLJ) offshore of the Chilean coast. This jet is frequent during spring and summer months, is strongest between 300 and 400 m above sea level, and is dynamically linked to the southeast Pacific anticyclone and coastal upwelling (Aguirre et al. 2019). Its structure and mechanics are similar to those of northerly low-level jets offshore of the California (U.S.) west coast. During winter, the Chilean southerly LLJ is not as frequent as it is in summer, partly because northerly (poleward) low-level jets sometimes develop in advance of the passage of mid-latitude disturbances and cold fronts. Only a few studies (Barrett et al. 2009; Viale and Norte 2009; Barrett et al. 2011) have described these northerly low-level jets, and those authors have found that they develop as "barrier jets" as a result of mountain flow blocking when Froude numbers are less than 1.0. However, those studies did not delve into the structure or mechanics of the northerly low-level jet in Chile. It is thus a topic that needs further study, particularly to compare and contrast it with other LLJs known to impact severe convection, such as the low-level jet that forms to the east of the Rocky Mountains (Chen and Kpaeyeh 1993; Squitieri and Gallus 2016).

Because wind shear and SRH depend strongly on the change in wind direction and speed in the lower troposphere (Thompson et al. 2007), barrier jets that develop in response to flow blocking by the Andes could possibly act to enhance the mesoscale conditions favorable for severe thunderstorms and tornado formation. This enhancement to SRH and wind shear by the low-level flow was seen for tornadoes in the lee of the Appalachian Mountains (LaPenta et al. 2005), adjacent to the topography in Greece (Matsangouras et al. 2014; Matsangouras et al.

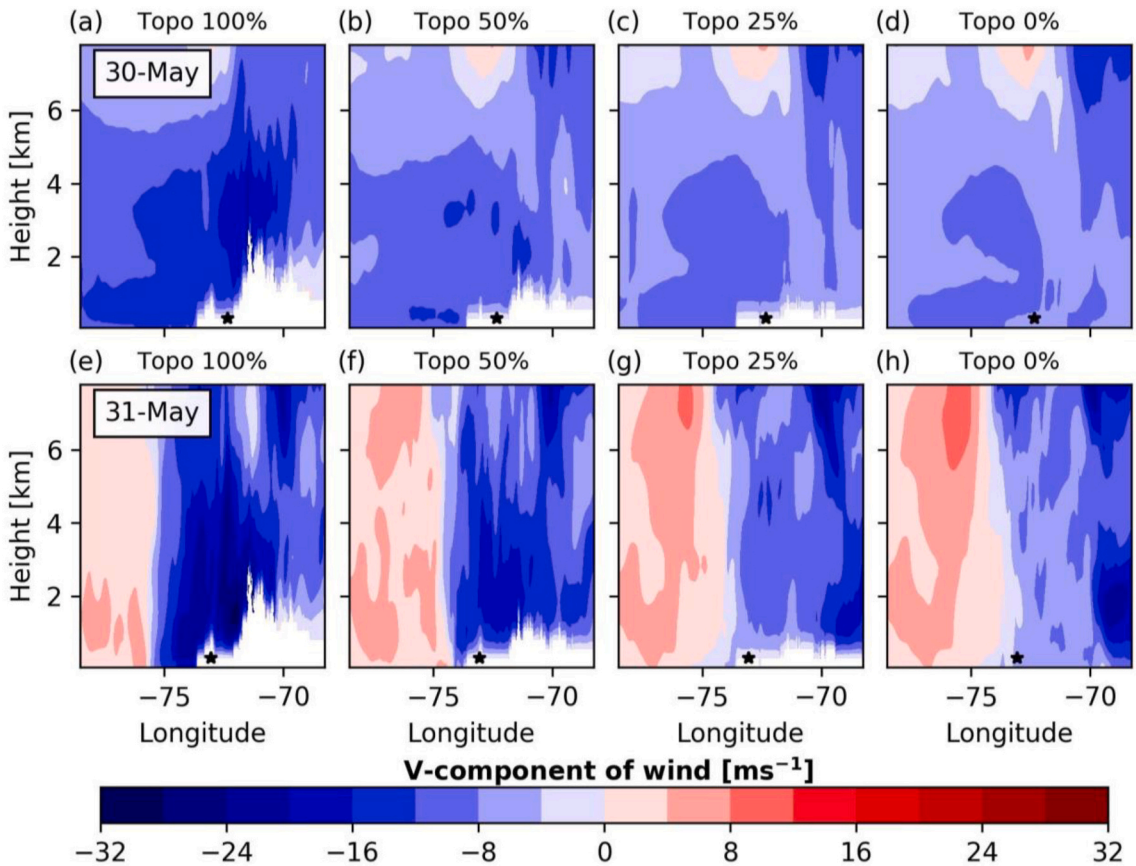

Fig. 4. Height-longitude cross-section of the meridional wind component at 37°S latitude for (a) the CTRL, (b) Sim_50p, (c) Sim_25p, and (d) Sim_0p simulations for 30 May 2019 at 2150 UTC (1750 LT), and the same in (e)-(h) except for 31 May 2019 at 1800 UTC (1400 LT). Black stars show the locations of the cities of Los Angeles (30 May) and Concepción (31 May).

2016), in the Mohawk Valley of New York (Tang et al. 2016), and upstream of the Sierra Nevada Mountains of California (Hanstrum et al. 2002). Given the frequency and intensity of northerly barrier jets upstream of the Andes (Viale and Nuñez 2011), it is possible that the topography contributed to the tornado formation on 30 and 31 May 2019. B20 used coarse-resolution reanalysis and a higher-resolution Weather Research and Forecasting (WRF) simulation to examine the presence of such a barrier jet and concluded that it may have played a role in enhancing vertical wind shear in the lower troposphere. However, they did not explore the jet further or run any sensitivity experiments. This study aims to use a number of high-resolution numerical sensitivity experiments to analyze the role of the Andes topography in generating this barrier jet and its contribution to conditions favorable for severe thunderstorm and tornado formation.

Sea-surface temperatures have also been shown to affect tornado formation in different cases around the world. For example, Molina et al. (2016) and Molina et al. (2018) found that warmer sea surface temperatures in the Gulf of Mexico increased CAPE over the central and southeastern U.S. and thus led to more frequent tornado activity there. Miglietta et al. (2017) used the WRF model to confirm that above-normal SSTs in the Mediterranean Sea helped strengthen a tornado-producing supercell storm that impacted southern Italy. Finally, Molina and Allen (2019) noted that lower-troposphere parcel trajectories from regions with above-normal SSTs led to more moist surface conditions that favored tornadoes in the U.S. In Chile, above-normal SSTs in autumn and winter have been related to circulation and precipitation extremes, including on the planetary scale (Aceituno 1993; Montecinos and Aceituno 2003; Barrett and Hameed 2017), synoptic-scale (Rutllant and Fuenzalida 1991), and mesoscale (Barrett et al. 2016; Bozkurt et al. 2016). However, because severe convective storms are relatively rare events in Chile (Brooks et al. 2003), there are no studies that examine how SSTs might influence the severity of convection in Chile, particularly in the cool season. One study examining cool-season (May–-September) tornadoes in Australia concluded that anomalies in local SSTs - which are typically low, around 15 °C, during the cool season - do not have much influence on tornadoes there (Kounkou et al. 2009). However, buoyancy from post-frontal cool air moving over a relatively warm sea surface may generate locally strong low-level vertical accelerations. Both V19 and B20 noted a synoptic-scale region of above-normal SSTs (1–2 °C) over the east-central southeast Pacific during the last week of May 2019, coinciding with the two tornado days, but neither examined the possible contribution of the SSTs to the conditions favorable for severe thunderstorm and tornado development. This study also aims to fill that gap.

To summarize, the primary goal of this study is to better understand two of the physical mechanisms that led to severe thunderstorm and tornado formation: low-level wind shear (possibly aided by the Andes topography) and instability (possibly aided by SSTs over the southeastern Pacific Ocean). To do so, we perform a series of sensitivity studies using an advanced numerical weather prediction model (WRF Version 4.1.5; Skamarock et al., 2019). The remainder of this article is organized as follows: section 2 presents a brief overview (time of occurrence, path, duration, damage, main synoptic features) of the two tornadoes reported in south-central Chile on 30–31 May 2019, and section 3 describes the configurations of the different regional simulations performed to examine the sensitivity of the local atmospheric conditions, including possible flow blocking, during 30 and 31 May 2019 to the topography configuration and SST distribution. Section 4 presents and interprets the results of the simulations, and a discussion and conclusions are presented in section 5.

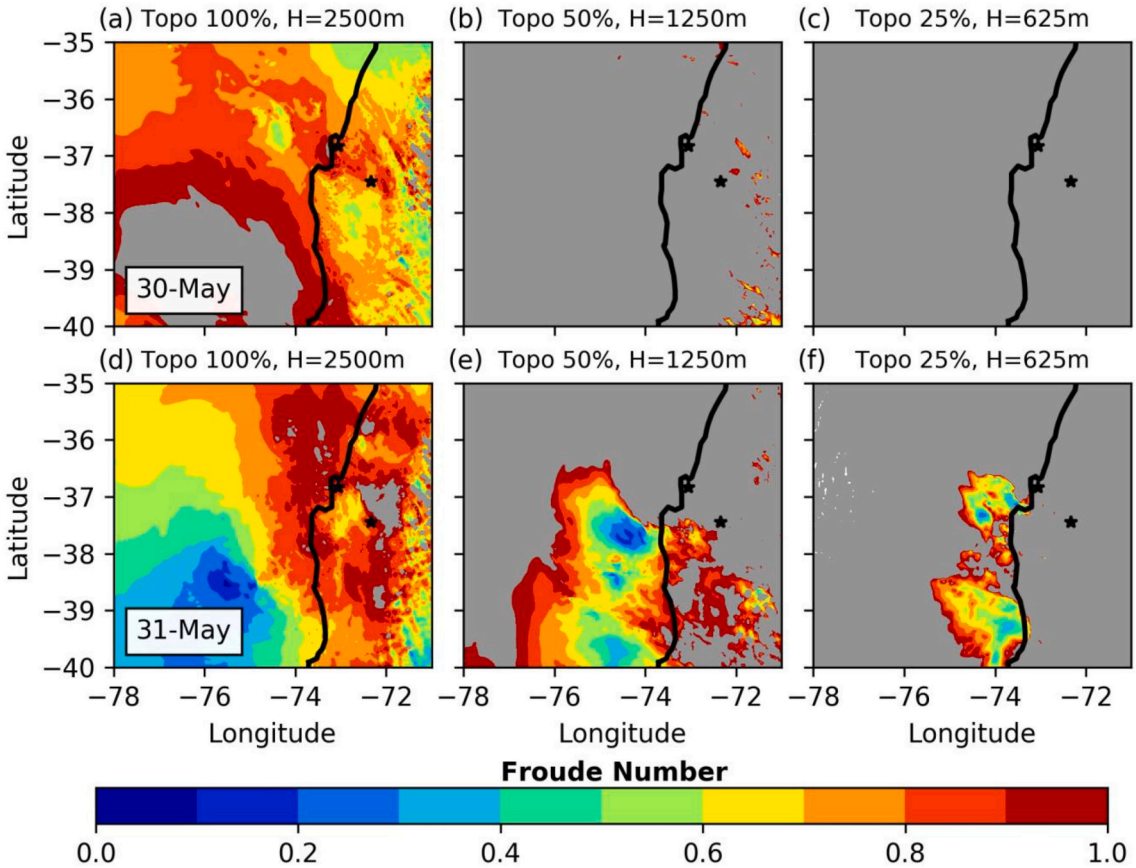

Fig. 5. Moist Froude number (*Frm*) at each grid-point of WRF domain d02 for (a) the CTRL, (b) Sim_50p, and (c) Sim_25p simulations for 30 May 2019 at 2150 UTC (1750 LT), and the same in (d)-(f) except for 31 May 2019 at 1800 UTC (1400 LT). Black stars show the locations of the cities of Los Angeles and Concepción. Gray areas represent *Frm* values larger than 1.0.

2. Overview of the tornado cases on 30 and 31 May 2019

On 30 May 2019 from approximately 2157–2205 UTC (1757–1805 local time), a tornado was observed in the city of Los Angeles, Chile (population approximately 130,000, altitude 140 m above sea level, 37.45°S, 72.33°W) by multiple residents, several of whom filmed portions of it and shared those videos on social media platforms. Based on damage surveys conducted after its passage, a formal report by the DMC (V19) estimated that the cyclonically rotating tornado moved primarily in a north-northwest to south-southeast curved path of around 5 km that lasted 7–8 min (Fig. 1a). The tornado was rated EF-2 (wind speeds 178–217 km hr^{-1}) on the enhanced Fujita scale. On 31 May 2019, another tornado, which first developed offshore, moved through the twin cities of Talcahuano and Concepción, Chile (population approximately 1.3 million, altitude 10–30 m above sea level, 36.82°S, 73.05°W). The official DMC analysis estimated that the tornado lasted 15 min from 1800 to 1815 UTC (1400–1415 local time) and had a curved path of around 18 km, also moving primarily from northwest to southeast (Fig. 1b). Multiple residents also filmed this event, similar to the tornado the day before, and those videos can also be found on social media platforms. The official report concluded the tornado in Talcahuano/Concepción had a maximum intensity of EF-1 (wind speeds between 138 and 177 km hr^{-1}). The Ministry of Housing and Urbanism estimated that more than one hundred homes suffered damage as a result of the passage of both tornadoes in the region.

The study of B20 determined that both tornadoes developed under an anomalous mid-troposphere trough at 500 hPa located to the west of Chile, in a post-frontal environment with a cyclonic low-level jet centered near 850 hPa and a surface low pressure located along the coast. Above-normal sea-surface temperatures (SSTs) were present over large areas of the southeast Pacific Ocean (anomalies of +1–2 °C in an region with climatological values of 11–16 °C) and the coastal zone adjacent to south-central Chile (anomalies of +0.5 °C in a region with climatological values of 11–14 °C) (see also V19). Surface and lower-tropospheric winds around the low pressure system advected above-normal θ_e into the region on the days of each tornado. Above-normal values of surface-based CAPE, on the order of 500 J kg^{-1} (higher on 30 May and lower on 31 May), were associated with each tornado. Similarly, high values of low-level (0–1-km) and deep layer (0–6-km) bulk shear (both near 15 m s^{-1} on 30 May and 20 m s^{-1} on 31 May) were also present on each day. For a more detailed description and discussion of the conditions that supported severe thunderstorms and tornado formation on those days, we refer the reader to V19 and B20.

Table 2
Moist Froude number calculated from radiosondes at Santo Domingo using a characteristic height of 3 km. Dates in boldface indicate the times closest to the tornado occurrences.

Date	Santo Domingo
29-May 00 UTC	0.2
29-May 12 UTC	1.0
30-May 00 UTC	0.4
30-May 12 UTC	0.7
31-May 00 UTC	0.3
31-May 12 UTC	0.4
01-Jun 00 UTC	0.4
01-Jun 12 UTC	0.2

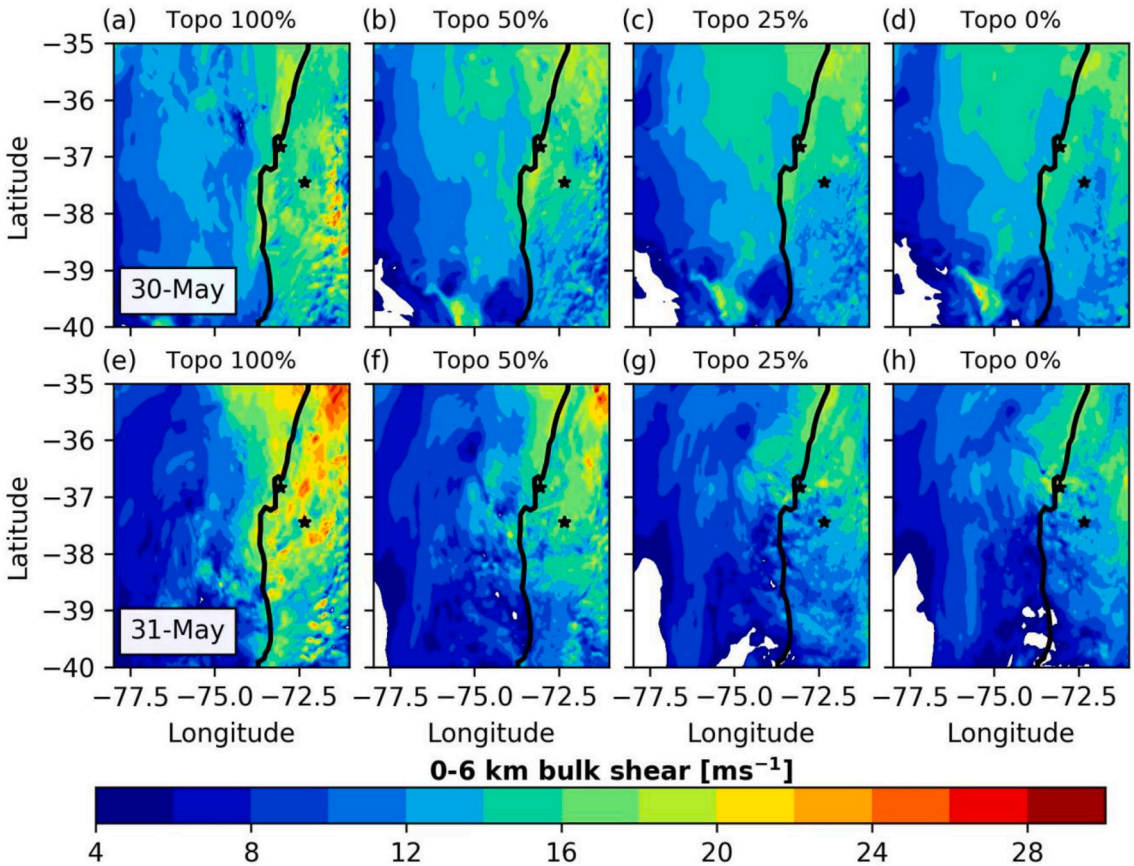

Fig. 6. The 0-6-km bulk shear (in m s^{-1}) for (a) the CTRL, (b) Sim_50p, (c) Sim_25p, and (d) Sim_0p simulations for 30 May 2019 at 2150 UTC (1750 LT), and the same in (e)-(h) except for 31 May 2019 at 1800 UTC (1400 LT). Black stars show the locations of the cities of Los Angeles and Concepción.

3. Data and methods

3.1. WRF model simulations

To better understand the role of the topography and SST in supporting those environments favorable for tornado formation, the output from nine simulations using the WRF model version 4.1.5 (Skamarock et al., 2019) was analyzed. A control (CTRL) simulation was performed using three nested domains with horizontal resolutions of 9, 3, and 1 km (Fig. 2a), 55 irregularly spaced vertical sigma levels, and a 50-hPa model top (a setup that was very similar to the simulation in B20). It was initialized at 0000 UTC 30 May 2019 (approximately 20 h prior to the first tornado) and ended at 1200 UTC 01 June 2019 (approximately 18 h after the second tornado). Initial and boundary conditions (every six hours) were provided by the National Centers for Environmental Prediction (NCEP) Final (FNL) analysis at 0.25° x 0.25°-degree horizontal grid spacing. Outputs from domains 2 and 3 were saved every five minutes and were used in the analysis of these tornado cases.

The simulation used the Thompson microphysics scheme (Thompson et al. 2008), the four-layer Noah-MP land surface model (Niu et al. 2011), the Rapid Radiative Transfer Model (RRTMG, Iacono et al. 2008) parameterization for shortwave and longwave radiation, and the Mellor-Yamada Nakanishi Niino (MYNN, Nakanishi and Niino 2006) Level 2.5 parameterization for the planetary boundary layer. Additionally, the Betts-Miller-Janjic (Janjic 1994) cumulus parameterization was used for the coarser domain (9 km), and no cumulus parameterization was applied to the inner two nested grids.

Three sensitivity simulations were conducted to analyze the impact of the topography on the mesoscale circulations local to each tornado (Fig. 2; Table 1). They only differed from the CTRL simulation in the topography used (see Table 1). In the first simulation (Sim_50p), the height of the topography was reduced to 50% of its original height; in the second simulation (Sim_25p), the height of the topography was reduced to 25% of its original height; and the third simulation was performed reducing the topography to 0% of its original height (Sim_0p). Terrain elevations in the CTRL, Sim_50p, and Sim_25p simulations are shown in Fig. 2a-c. In addition, height-longitude cross-sections at the latitude of the city of Concepción are also shown for CTRL, Sim_50p, and Sim_25p (Fig. 2d). The city of Los Angeles has a very similar height-longitude cross-section, being only 0.63° latitude to the south, so the cross-section shown in Fig. 2 is also representative of Los Angeles.

Three more simulations were performed to analyze the sensitivity of the mesoscale tornado environments to SSTs in the southeastern Pacific Ocean (Fig. 3a; Table 1). One simulation was performed reducing the SST by 2 °C (SST-2 K) uniformly over the three domains (Fig. 3b); another simulation was performed by increasing the SST by 2 °C (SST + 2 K) uniformly over the three domains (Fig. 3c); and a third simulation was performed with the goal of eliminating the strong SST gradient present to the northwest of the study region during 30 and 31 May 2019 (SST16C). The synoptic analysis conducted in B20 indicated the advection of large equivalent potential temperature values from the northwest. In addition, a relatively intense tongue of CAPE values was shown close to the coast on both days, extending from the northwest into the study region. Based on that, we aimed to investigate whether the intense SST gradient located to the northwest of the study region had some influence on the severity of storms that formed in those days. To reduce that gradient, any SST values greater than 16 °C were reduced to exactly 16 °C; this primarily occurred over the northwest parts of the three model domains (Fig. 3d). The temperature of 16 °C was chosen because that is approximately the maximum surface air temperature measured in Los Angeles and Concepción on the days of both

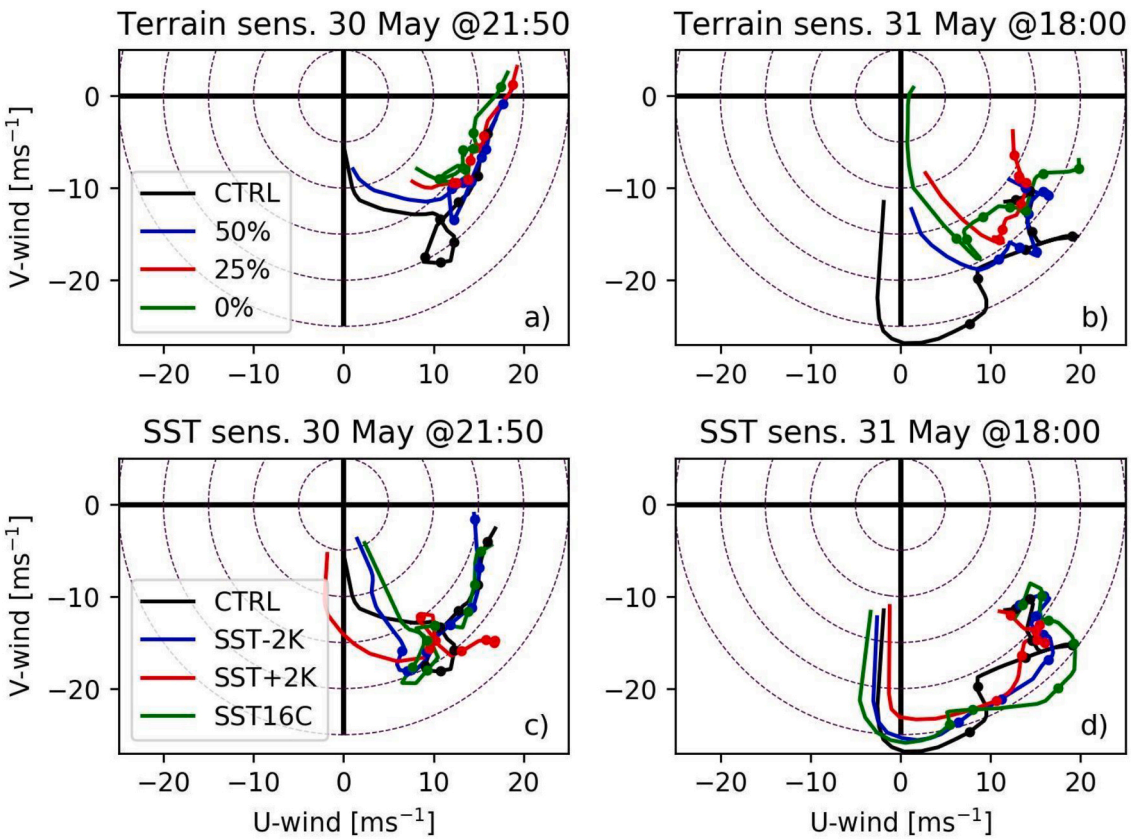

Fig. 7. Hodographs in the 0–7 km layer, where each dot represents 1 km of elevation (the surface conditions are plotted without a dot) of wind profiles over the city of (a,c) Los Angeles on 30 May 2019 at 2150 UTC and the (b,d) city of Concepción on 31 May 2019 at 1800 UTC from (a)-(b) sensitivity simulations to terrain height and (c)-(d) sensitivity simulations to SST distributions.

tornadoes (see V19 and B20). Two final simulations (for a total of eight sensitivity experiments) were performed to examine possible combined impacts of topography reduction and changes in SST. In the first of those (SST-2 K_0p), SST was reduced by 2 °C in all domains and topography was reduced to 0% of its original height. In the second simulation (SST + 2 K_0p), SST was increased by 2 °C in all domains and topography was reduced to 0% of its original height.

3.2. Flow blocking calculation

In order to estimate the degree of blocking of the cyclonic flow (see B20) by the Andes cordillera, we calculated the moist Froude number (*Frm*) following Chen and Lin (2005) using the expression:

$$Frm = \frac{U}{N_m H}$$

where H is the characteristic height of the Andes, U is the mean wind speed between 0–H km, and N_m is the unsaturated moist Brunt-Väisälä frequency, which was calculated following Emanuel (1994) using the expression:

$$N_m^2 = \frac{g}{\theta_V}\frac{d\theta_V}{dz}$$

where g is the gravitational acceleration (9.81 m s^{-2}) and θ_v is the virtual potential temperature. We calculated the *Frm* for radiosondes launched from Santo Domingo (located at 33.65°S, 71.61°W, approximately 400 km north of where the tornadoes occurred) at 0000 and 1200 UTC from 29 May to 01 June 2019. We also calculated the *Frm* using WRF output. A value of $H = 3$ km was used to calculate the *Frm* at Santo Domingo, and values of $H = 2.5$ km, 1.25 km and 0.625 km were used to calculate the *Frm* at each grid point in the WRF CTRL, Sim_50p, and Sim_25p simulations, respectively. We are aware that atmospheric conditions sampled by the radiosonde launched at Santo Domingo may not be representative of the environment where tornadoes formed. However, results from their analysis complement those from model simulations over the study region to support our claim that the synoptic-scale cyclonic flow was blocked by the Andes cordillera on 30–31 May 2019 ($Frm < 1.0$), helping to create conditions favorable for severe thunderstorm formation.

4. Results

In the following sections, we will show how the mesoscale conditions during the tornado events of May 30 and May 312,019 were affected by changes in terrain height (section 3.1) and SST (section 3.2). The goal here is to estimate the relative impact of these two factors on the vertical wind shear and instability present on those two days, and as a result, better understand the mechanisms that supported the organization and severity of the storms that generated the two tornadoes. In each subsection, the simulation results are presented first for 30 May 2019, then for 31 May 2019.

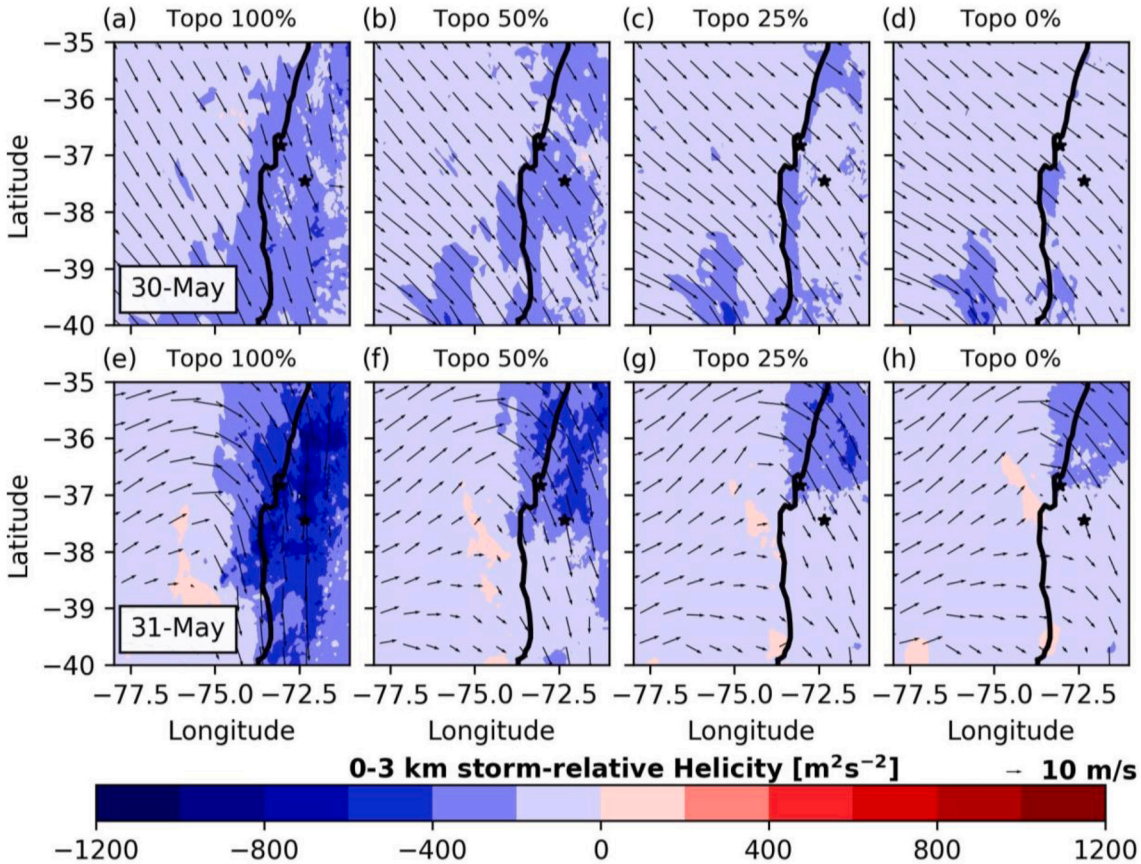

Fig. 8. The 0–3 km storm-relative helicity for (a) the CTRL, (b) Sim_50p, (c) Sim_25p, and (d) Sim_0p simulations for 30 May 2019 at 2150 UTC (1750 LT), and the same in (e)-(h) except for 31 May 2019 at 1800 UTC (1400 LT). Vectors represent the wind field at 900 hPa. Black stars show the locations of the cities of Los Angeles and Concepción.

4.1. Sensitivity to terrain height

4.1.1. Terrain height sensitivity on 30 May 2019

When the terrain was at its full height, height-longitude cross-sections of the meridional wind component at the time when the tornado was reported in the city of Los Angeles (2150 UTC or 1750 LT on 30 May 2019) show a strong northerly low-level jet over south-central Chile, with meridional winds greater than 18 m s^{-1} (Fig. 4a). When terrain height was progressively reduced to zero, the cross-sectional area encompassed by this northerly jet broadened, and magnitudes decreased to less than 10 m s^{-1} (Figs. 4b–d). This reduction in magnitude of wind speed with topography indicates that a significant part of the southward low-level jet shown by the CTRL simulation is likely caused by the Andes blocking the synoptic-scale northwesterly circulation associated with the surface, lower-, and mid-tropospheric trough located northwest of the study region on those days. This hypothesis was confirmed by moist Froude numbers (*Frm*) at each grid-point in the CTRL simulation ranging from 0.5–1.0 between 35°–37°S in the afternoon of 30 May 2019 (Fig. 5a). As the terrain height was reduced, *Frm* values were larger than 1.0 all over the domain (Figs. 5b-c), confirming that the flow was unblocked in the lower-terrain simulations. Farther north, moist Froude numbers (*Frm*) calculated from radiosondes launched at Santo Domingo were much lower than 1.0 from 29 to 30 May 2019 (Table 2). These observations, combined with results from the CTRL simulation, confirm that the low-level flow on 30 May 2019 was likely blocked by the Andes cordillera, and particularly so to the north of the city of Los Angeles. Nevertheless, the presence of relatively strong northerly flow even without topography (Fig. 4d) indicates that a fraction of the low-level jet was driven by synoptic-scale processes associated with the strong surface and lower troposphere cyclone. Both of these elements agree well with Barrett et al. (2009), who also noted substantial flow blocking in south-central Chile in advance of a mid-latitude cyclone that was reduced but not eliminated when topography was decreased.

The strong low-level northerly winds beneath westerly to northwesterly winds near 500 hPa in the CTRL simulation resulted in 0–6-km bulk shear values greater than 16 m s^{-1} over the city of Los Angeles (Fig. 6a) and its surroundings at 2150 UTC (1750 LT). The progressive

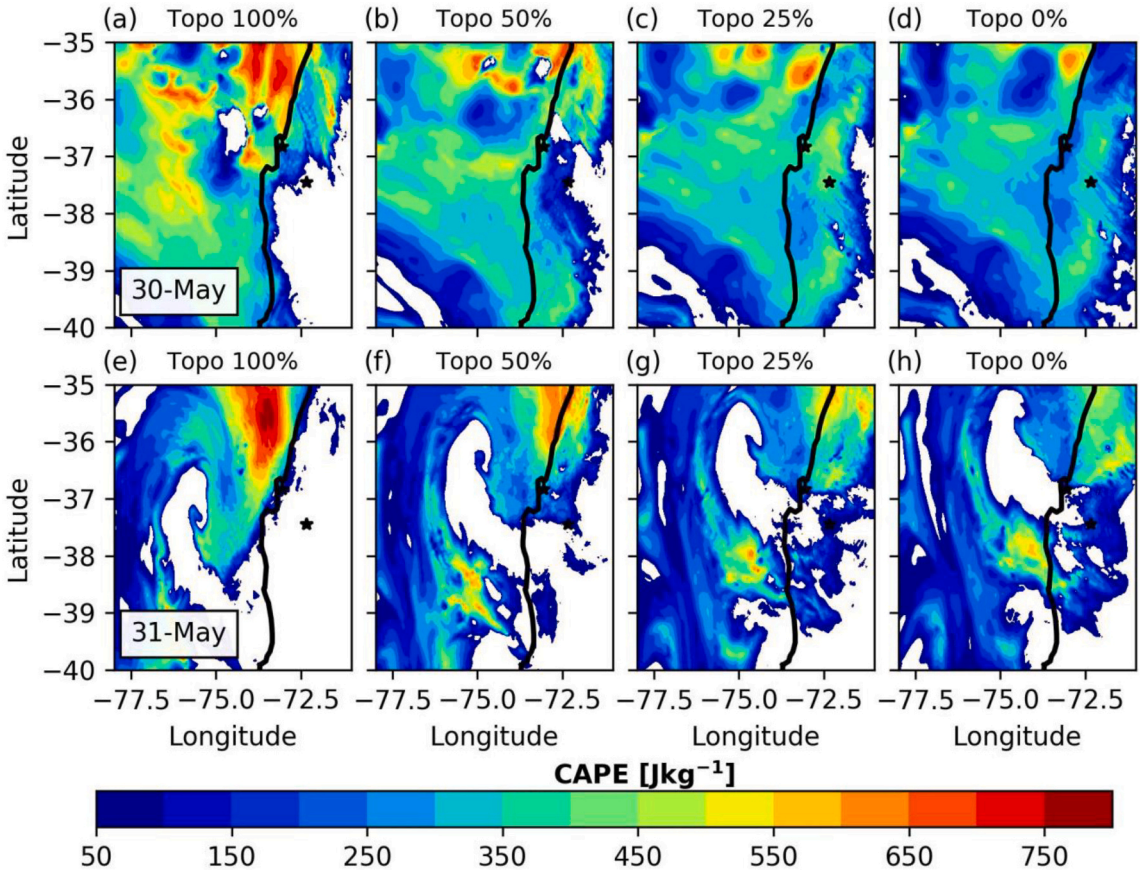

Fig. 9. The CAPE (in J kg^{-1}) for (a) the CTRL, (b) Sim_50p, (c) Sim_25p, and (d) Sim_0p simulations for 30 May 2019 at 2150 UTC (1750 LT), and the same in (e)-(h) except for 31 May 2019 at 1800 UTC (1400 LT). Black stars show the locations of the cities of Los Angeles and Concepción.

reduction of terrain height from 100% to 0% reduced the 0-6-km bulk shear (Figs. 6b–d), reaching values below 10 m s^{-1} in the simulation with zero terrain height (Fig. 6d). This reduction in 0–6-km bulk shear would have significant and negative consequences to storm organization and severity, in agreement with Rasmussen and Blanchard (1998) and Thompson et al. (2003). Composite studies suggest 0–6-km bulk shear values of 15–20 m s^{-1} are a lower bound for supercell thunderstorms (Rasmussen and Blanchard 1998; Houston et al. 2008). Indeed, Thompson et al. (2007) found a bulk shear of 10 m s^{-1} to be the 10th percentile value, meaning that 90% of all supercells had 0–6-km bulk shear values greater than 10 m s^{-1} (note that Thompson et al. 2007 used a slightly different definition of bulk shear, "effective bulk shear," to account for the storm-specific environment). This reduction in bulk shear is especially problematic for storms that form in environments with weak CAPE (< 500 J kg^{-1}), as they may need even *more* vertical wind shear to become supercellular and tornadic (e.g., Markowski and Straka 2000). Thus, the presence of greater bulk shear values when the topography is higher suggests that flow blocking by the Andes cordillera aids in conditioning the environment to favor severe thunderstorms and tornadoes.

Hodograph plots of wind profiles in model simulations at the nearest grid-point to the city of Los Angeles at 2150 UTC (1750 LT) indicate that the winds in the CTRL simulation largely increased with height in the 0–3-km layer, with a maximum around 3 km, turning counter-clockwise from northerly to a northwesterly direction in the layer from 0 to 6 km (Fig. 7a), a profile that favors not only the severity of storms but also tornadogenesis (Markowski and Richardson 2009, 2014). Following the Bunker (2000) methodology, a left-moving supercell in the CTRL environment would move at 13.9 m s^{-1} towards 119° (towards the southeast) with -253 m^2 s^{-2} of 0–3 km SRH (Fig. 8a; values are negative because the cyclonic rotation is in the Southern Hemisphere) and -163 m^2 s^{-2} of 0–1-km SRH (not shown). Hodographs from simulations with reduced topography showed less increase in wind speed with height and a more veered (westerly) wind direction in the 0–3-km layer (Fig. 7a), likely related to reduced blocking, resulting in smaller hodographs and particularly so in the lowest 3 km of

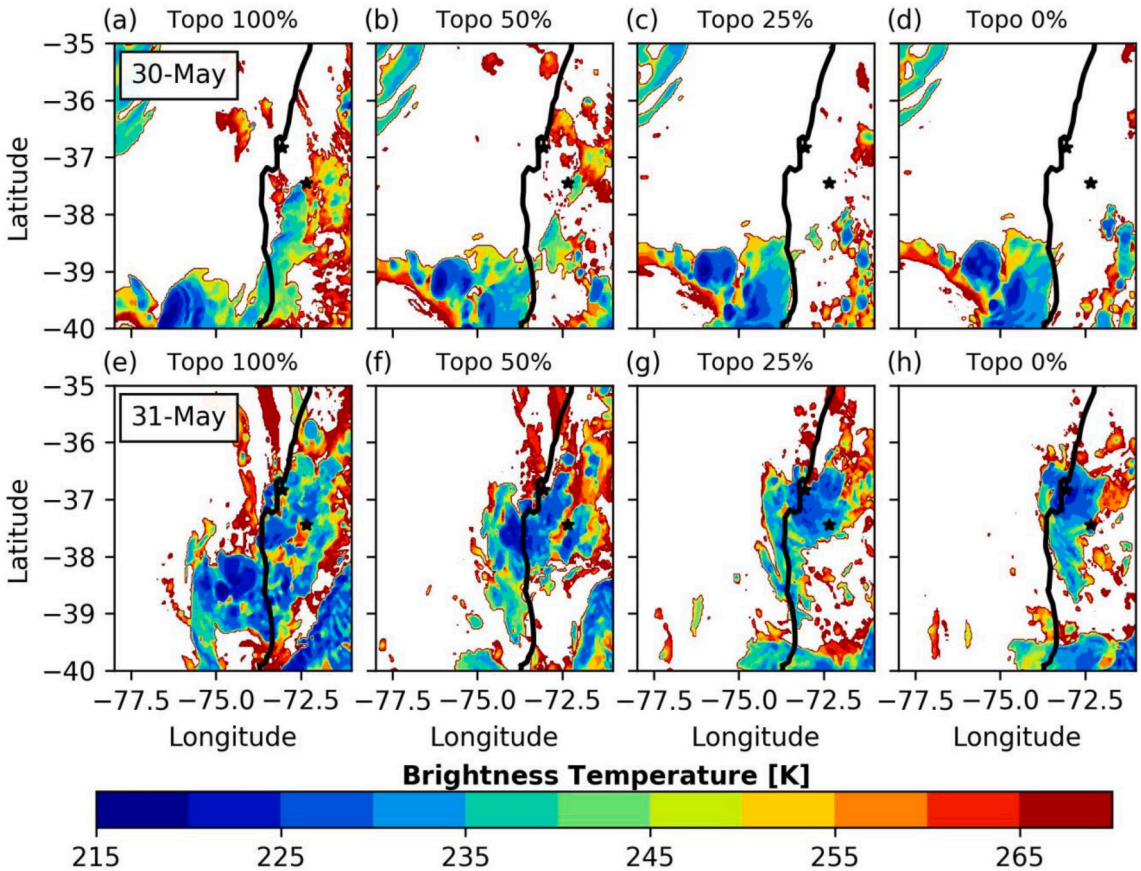

Fig. 10. Simulated infrared brightness temperature (in K) for (a) the CTRL, (b) Sim_50p, (c) Sim_25p, and (d) Sim_0p simulations for 30 May 2019 at 2150 UTC (1750 LT), and the same in (e)-(h) except for 31 May 2019 at 1800 UTC (1400 LT). Black stars show the locations of the cities of Los Angeles and Concepción.

the troposphere. Moreover, in those environments of reduced winds in the 0–6-km layer, storm motion would be slower (Bunkers et al., 2000); thus storm-relative winds would be weaker, and storm-relative helicity (SRH) would also be smaller. As a result, the 0–3-km SRH reduced (Figs. 8b-d) to near $-130\,\mathrm{m^2\,s^{-2}}$ without any topography. Note that even without topography, the cyclonic circulation around the synoptic-scale cyclone resulted in non-zero SRH, implying that the Andes aid but are not the sole factor in creating an environment favorable for tornadogenesis. Also note that all topography sensitivity simulations on 30 May 2019 had similar wind speed and direction at 7 km (Fig. 7a), indicating that the topography is important in augmenting wind shear in the lower (but not necessarily middle) troposphere. The wind field at 900 hPa in the CTRL and terrain sensitivity simulations (Figs. 8a-d) also indicates less blocking as the terrain height is reduced, thus allowing the air masses to more freely flow to the east.

While instability might not be thought to be related to changes in topography, in this case, it turns out that CAPE was adjusted by changes in wind speed and direction associated with the reduction in topography. When terrain height was reduced, CAPE values in the inland region surrounding Los Angeles generally increased by about $100\,\mathrm{J\,kg^{-1}}$ for each 25% that terrain height was reduced (Figs. 9a–d). In this study, CAPE values were calculated using a surface-based parcel, and so all future references to CAPE are to surface-based CAPE. This inverse relationship between CAPE and topography height may be due to the combination of two factors. First, without the Andes to act as a barrier, there appears to have been greater inland advection of relatively warm and humid surface air from the southeast Pacific, as seen by surface and lower-tropospheric winds more from the west and northwest in the lower-terrain simulations (Fig. 7a) compared to coast-parallel northerly winds in the full-topography simulation. That warmer and more humid surface air would contribute to greater CAPE. Second, both convective and stratiform cloudiness was reduced inland

with decreasing terrain height (Figs. 10a–d), allowing more solar radiation to reach the surface and thus increasing surface temperatures and CAPE. Cloud cover may have been reduced by eliminating the downstream mountain barrier that is known to generate cloudiness on its upslope side (Viale and Garreaud 2015), and also by allowing any clouds and convection to disperse to the east into Argentina (Figs. 10b–d).

Even though CAPE was generally 100–300 J kg^{-1} lower in the CTRL simulation over land and actually increased with decreased topography, there are still more swaths of 2–5-km layer updraft helicity (a diagnostic designed to indicate updraft rotation in simulated storms; Clark et al. 2013) in the CTRL than in the other simulations in the four-hour time window 1950–2350 UTC on 30 May 2019 (Figs. 11a–d). (Note updraft helicity is negative for cyclonically rotating storms because we are in the Southern Hemisphere). These swaths steadily decreased in number and magnitude as the terrain height was reduced (Figs. 11b–d), pointing to fewer rotating updrafts. This indicates that on 30 May 2019, the positive effects from greater shear aided by the full Andes topography outweighed the negative effects from reduced CAPE that resulted when the topography was at its fullest height. In summary, in the CTRL simulation (with the full Andes cordillera) on 30 May 2019, deep convection was more frequent, magnitudes of 0–6-km bulk shear were greater, lower-tropospheric winds were faster and more northerly, and 0–3-km SRH was greater, all of which were conditions that favored rotating, potentially tornadic thunderstorms. These results indicate that the Andes topography aided in creating conditions that were favorable for severe thunderstorms and the tornado that day.

4.1.2. Terrain height sensitivity on 31 May 2019

On 31 May 2019 at 1800 UTC (1400 LT), when a tornado was reported in the cities of Talcahuano and Concepción, height-longitude vertical cross sections in the CTRL simulation showed an even stronger lower-troposphere northerly wind component (when compared to the day before; Fig. 4a) on the western slopes of the southern Andes Cordillera (Fig. 4e). As was indicated by B20, this stronger northerly wind value produced larger 0–6-km bulk shear (21.4 m s^{-1} in Concepción; Fig. 6e) than the day prior. Just as on 30 May 2019, as terrain heights were reduced, low-level northerly winds on 31 May 2019 decreased

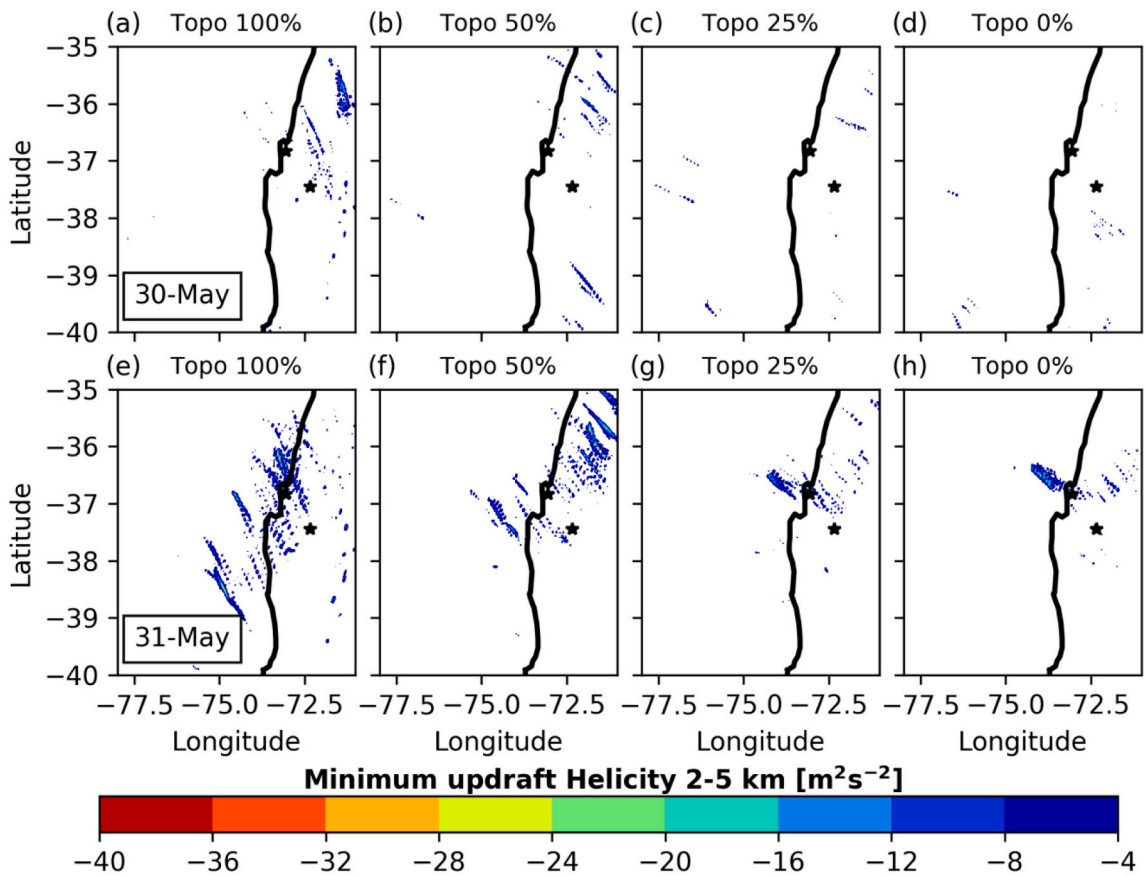

Fig. 11. Minimum model updraft helicity in the 2–5 km layer (color shaded; m^2 s^{-2}) for (a) the CTRL, (b) Sim_50p, (c) Sim_25p, and (d) Sim_0p simulations for the period 1950–2350 UTC (1550–2150 LT) 30 May 2019, and the same in (e)-(h) except for 1600–2000 UTC (1200–1600 LT) 31 May 2019. Black stars show the locations of the cities of Los Angeles and Concepción.

(Figs. 4f-h) and bulk shear values came down (Figs. 6f-h), reducing to less than 15 m s^{-1} for the 0% simulation. The impact on hodographs from 31 May 2019 was similar (Fig. 7b): as terrain height was reduced, lower-tropospheric winds over Concepción were weaker and showed less counter-clockwise turning with height in the 0–6-km layer, resulting in smaller hodographs and less vertical wind shear.

Similar to 30 May 2019, Froude numbers of 0.4 were calculated from the 1200 UTC 31 May 2019 and 0000 UTC 01 June 2019 Santo Domingo radiosondes (Table 2). Froude numbers calculated from the CTRL simulation were larger than those from the day before, but were still generally lower than 1.0 between 35°–37°S (Fig. 5d), thereby confirming flow blocking by the full Andes topography. Froude numbers increased to values larger than 1.0 as terrain height was reduced (Figs. 5e–f). As topography was reduced, the eastward wind component on 31 May 2019 increased (Figs. 5d–f, 8e–h).

The 0–3-km storm-relative helicity was largest in the CTRL simulation (Fig. 8e), and as the terrain height was reduced, SRH weakened from more than $-600\,m^2\,s^{-2}$ to less than $-200\,m^2\,s^{-2}$ (Figs. 8g–h). Similar to 30 May 2019, the significant changes in 0–6-km bulk shear and 0–3-km SRH on 31 May 2019 highlight the importance of the topography in generating low-level wind shear that favored rotating storms and tornadoes. This is confirmed in horizontal distributions of the minimum 2–5-km updraft helicity: as topography is reduced, the number and concentration of swaths of southeastward-moving updraft helicity cells is reduced (Figs. 11f–h) when compared to the CTRL (Fig. 11e).

The impact of topography on CAPE was also investigated for 31 May 2019. The horizontal distribution of CAPE in the CTRL simulation showed a region of relatively large values (> 750 J kg^{-1}) approaching the coast and the city of Concepción from the northwest, embedded in the low-level cyclonic circulation (Fig. 9e). The reduction of terrain height resulted in the displacement of this "tongue" of relatively large CAPE values inland and to the east (Figs. 9f-h), resulting in an inverse relationship between inland CAPE and topography height, similar to 30

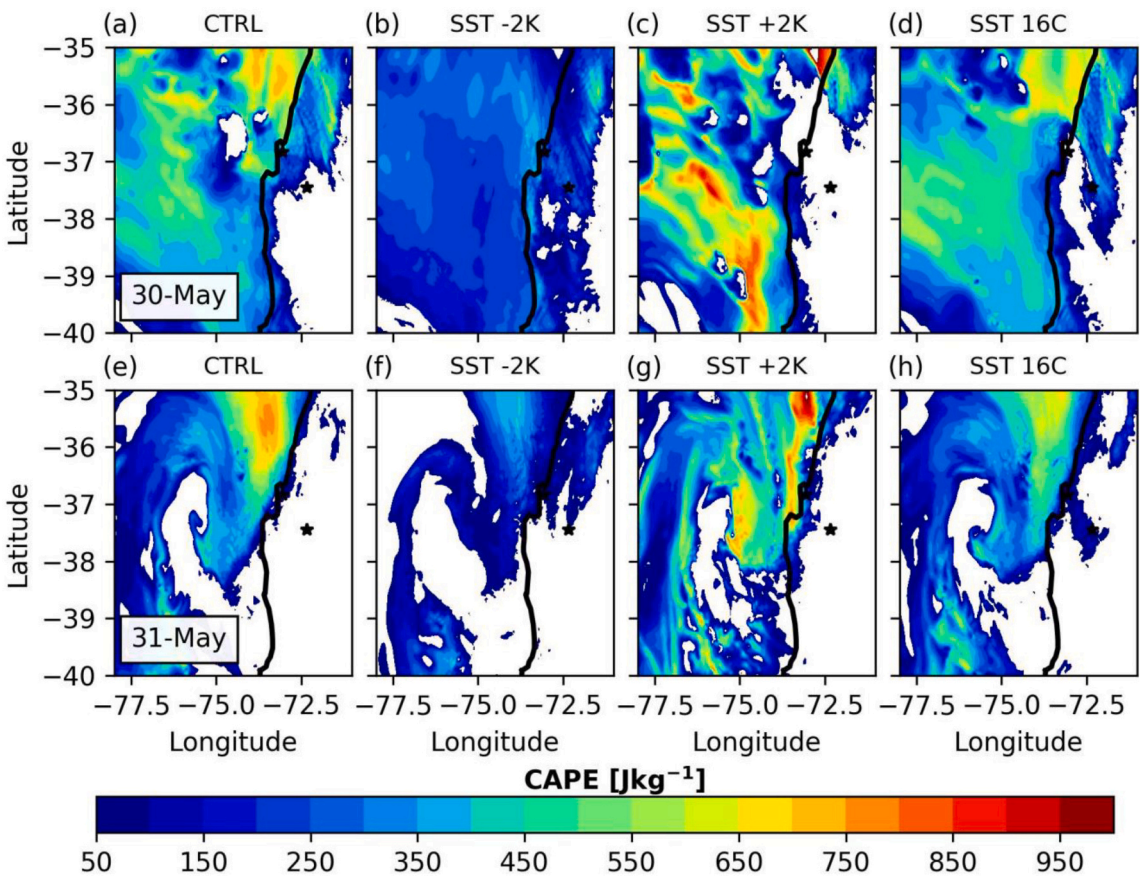

Fig. 12. The CAPE (in J kg^{-1}) for (a) the CTRL, (b) SST-2 K, (c) SST + 2 K, and (d) SST16C simulations for 30 May 2019 at 2150 UTC (1750 LT), and the same in (e)-(h) except for 31 May 2019 at 1800 UTC (1400 LT). Black stars show the locations of the cities of Los Angeles and Concepción.

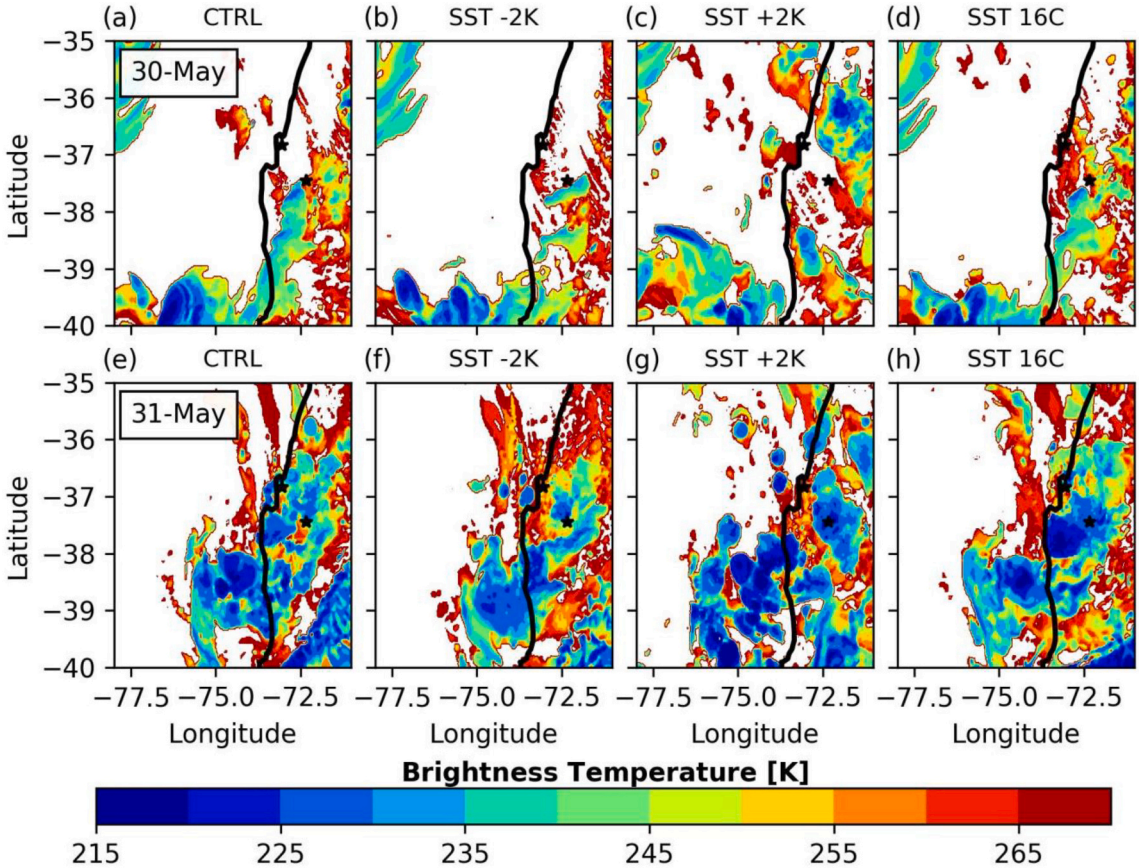

Fig. 13. Simulated brightness temperature (in K) for (a) the CTRL, (b) SST-2 K, (c) SST + 2 K, and (d) SST16C simulations for 30 May 2019 at 2150 UTC (1750 LT), and the same in (e)-(h) except for 31 May 2019 at 1800 UTC (1400 LT). Black stars show the locations of the cities of Los Angeles and Concepción.

May 2019. However, although CAPE increased inland as topography height decreased, the relative lack of updraft helicity swaths (Figs. 11e–f) and convection (Figs. 10e–f) as the topography was decreased suggests that the increase in vertical wind shear is again more important than the decrease in CAPE to favor rotating storms and tornadoes. This result is similar to other regions of the world where shear is more important than CAPE for tornado activity (Brooks et al. 2003; Groenemeijer and van Delden 207; Thompson et al. 2007; Clark 2009; Grünwald and Brooks 2011; Wesolek and Mahieu 2011; Sherburn and Parker 2014; Sherburn et al. 2016; Sherburn et al. 2016; Barrett et al. 2020).

4.2. Sensitivity to SST

4.2.1. SST sensitivity on 30 May 2019

When sea-surface temperatures were adjusted, CAPE values offshore and over the coast of south-central Chile at the time of the tornado occurrence on 30 May were generally higher (approaching 1000 J kg^{-1}, or 200–800 J kg^{-1} greater) in the warmer (SST + 2 K) simulation (Fig. 12c) than either the CTRL (Fig. 12a) or the other two simulations. In the cooler (SST-2 K) simulation, offshore CAPE (Fig. 12b) was between 200 and 400 J kg^{-1} lower than the CTRL. CAPE values in the SST16C simulation were very similar to the CTRL (Fig. 12d). Thus, offshore instability was higher in simulations with warmer SSTs and lower in simulations with cooler SSTs. Inland instability values were more complex to analyze, as an increase in the coverage of convection when SSTs were warmed (Fig. 13) likely reduced the CAPE available at the moment of the tornado (2150 UTC). Thus, *inland* CAPE values were actually highest in the coolest simulations (SST-2 K and SST16), despite the warm SST simulation (SST + 2 K) having higher values of *offshore* CAPE. The effect of this CAPE variability on storm coverage and intensity across the four simulations can be seen in the spatial distribution of minimum updraft helicity in the 2–5-km layer (Fig. 14). Updraft helicity swaths were greatest in intensity (negative values) and longitude in the warm simulation (SST + 2 K; Fig. 14c), and weakest in intensity and shortest in duration in the cool simulation (SST-2 K;

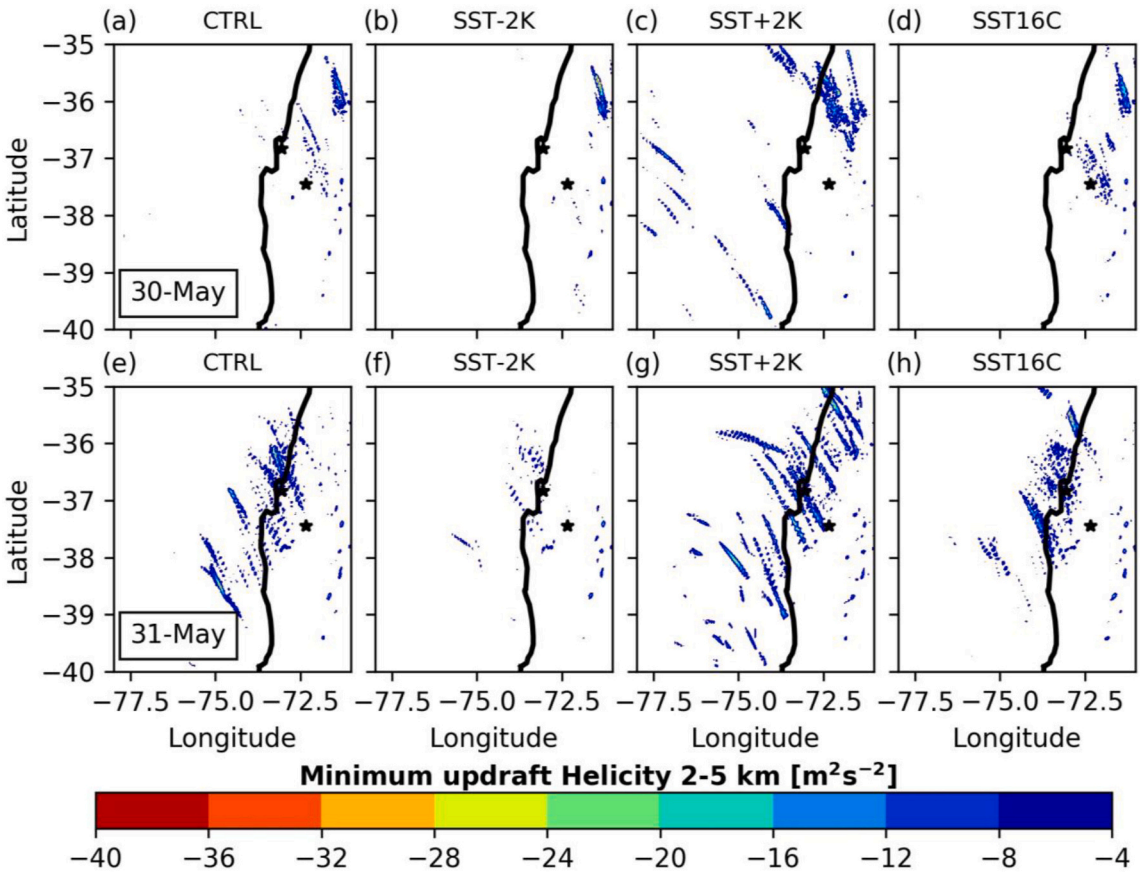

Fig. 14. Minimum model updraft helicity in the 2–5 km layer (color shaded; $m^2\ s^{-2}$) for (a) the CTRL, (b) SST-2 K, (c) SST + 2 K, and (d) SST16C simulations for 1950–2350 UTC (1550–2150 LT) 30 May 2019, and the same in (e)-(h) except for 1600–2000 UTC (1200–1600 LT) 31 May 2019. Black stars show the locations of the cities of Los Angeles and Concepción.

Fig. 14b). Furthermore, convection appeared to be more intense (characterized by colder brightness temperatures) in the warm simulation (Fig. 13c) compared to the CTRL, and convection in the cold simulation (Fig. 13b) appeared to be least numerous and weakest (warmest brightness temperatures) of any of the SST simulations. This pattern suggests that warmer SSTs favored both a larger number of convective storms and more intense convection, while colder SSTs favored less and less-intense convection. Brightness temperature in the SST16C simulation was very similar to the CTRL (Fig. 13d), suggesting that the warm SSTs more than 500 km to the northwest of south-central Chile had little impact on local convection intensity on 30 May 2019.

While vertical wind shear might not be thought to be related to changes in SST, in this case, it turns out that vertical wind shear can be adjusted by changing SST. When SSTs were warmed (SST + 2 K), 0–6-km bulk shear increased by 2–4 $m\ s^{-1}$ over the inland portions of south-central Chile (Fig. 15c). When SSTs were cooled everywhere (SST-2 K) and when they were reduced to 16 °C (SST16C), 0–6-km bulk shear resembled the CTRL simulation (Figs. 15a,b,d). The increase in bulk shear in the warm simulation appears to be related to changes in surface and 6–km winds in the warm simulation when compared to the CTRL (compare the red and black curves in Fig. 7c). The physical reasons behind these changes in wind were not explored in this study and remain an open question. Hodographs for the other SST simulations largely resembled the CTRL simulation (Fig. 7c), supporting the similar magnitudes of 0–6-km bulk shear (Fig. 15). Inland magnitudes of 0–3-km SRH strengthened by $-100\ m^2\ s^{-2}$ in the warm simulation (SST + 2 K) compared to the CTRL (Figs. 16a,c), while magnitudes of SRH in the cold simulation (SST-2 K) weakened by up to $+200\ m^2\ s^{-2}$ (Fig. 16b). As reported earlier, updraft helicity swaths and convective coverage and intensity were greatest in the warm simulation (Figs. 13c and 14c), but it is unclear if the contribution to that increase came more from the increase in CAPE or the increase in shear. The cold SST simulation showed the least number of updraft helicity swaths and the weakest and smallest area of convective storms (Figs. 13b and 14b),

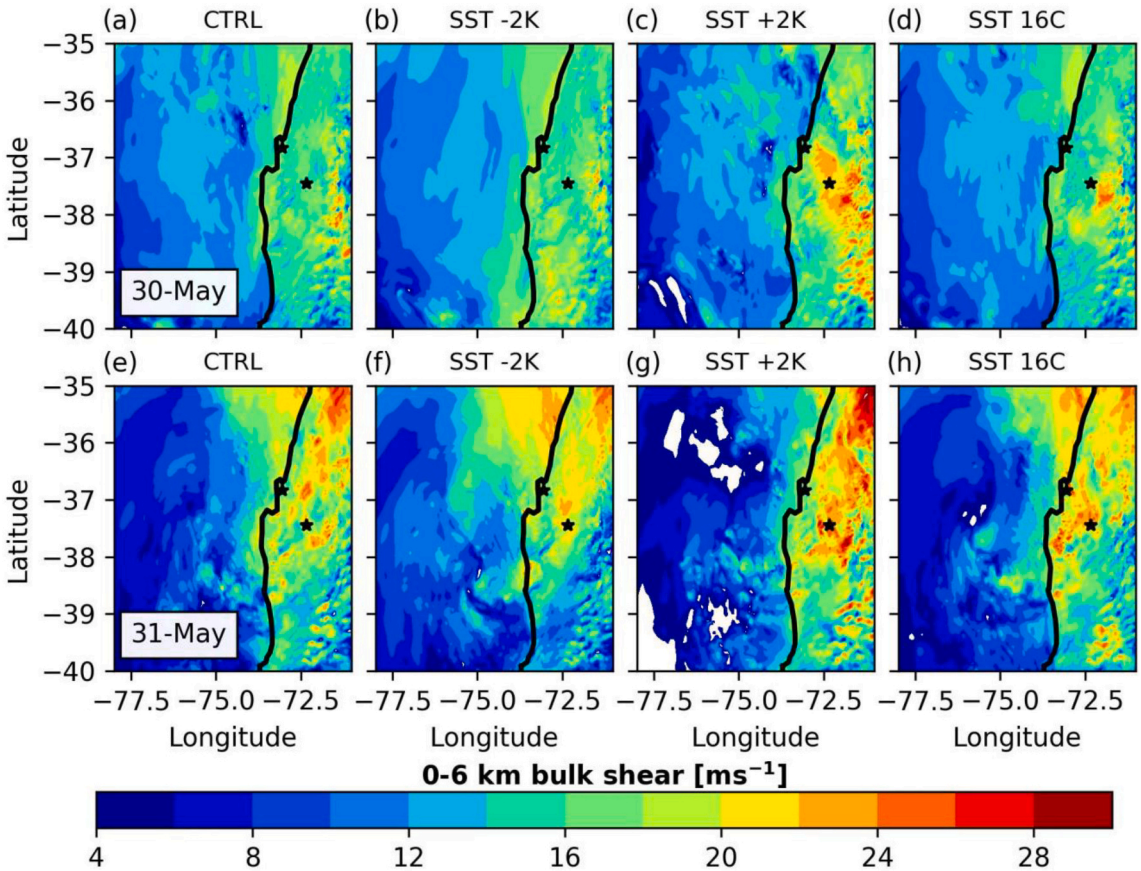

Fig. 15. The 0–6 km bulk shear (in m s^{-1}) for (a) the CTRL, (b) SST-2 K, (c) SST + 2 K, and (d) SST16C simulations for 30 May 2019 at 2150 UTC (1750 LT), and the same in (e)-(h) except for 31 May 2019 at 1800 UTC (1400 LT). Black stars show the locations of the cities of Los Angeles and Concepción.

despite having similar environmental SRH and bulk shear values as in the CTRL simulation. This suggests that in the cold simulation, the reduction in CAPE was the primary contributor to the decrease in convective intensity and coverage.

4.2.2. SST sensitivity on 31 May 2019

On 31 May 2019, the warmer simulation (Fig. 12g) had near-coast CAPE values 200–400 J kg^{-1} higher than the CTRL (Fig. 12e), while the colder simulation (Fig. 12f) had near-coast CAPE values 200–400 J kg^{-1} lower than the CTRL. Reducing the SST to 16 °C lowered the offshore CAPE values (more than 200 km northwest of the coast) by 200 J kg^{-1} (Fig. 12h) compared to the CTRL, but did not lower the CAPE values at the immediate coast. The impacts of these changes in CAPE in all three simulations are seen in both brightness temperatures (Figs. 13e–h) and updraft helicity (Figs. 14e–h). When CAPE is higher (SST + 2 K and CTRL), predicted helicity swaths are more intense and more numerous, and brightness temperatures are colder; when CAPE is lower, the reverse is seen.

The impacts of changing SSTs on vertical wind shear on 31 May 2019 were similar to 30 May 2019, in that the signals are generally mixed. The warmer simulation yielded greater values of inland 0–6-km bulk shear (Fig. 15g) than the CTRL simulation (Fig. 15e), but all four simulations had similar magnitudes of 0–3-km SRH around the city of Concepción (Figs. 16e–h). The hodograph on 31 May 2019 for warming SSTs showed backing and slowing of the lower-troposphere winds (which could act to reduce vertical wind shear). However, that backing and slowing was opposite of the pattern seen for the warm simulation on 30 May 2019 (compare red curves in Fig. 7c and d). Thus, it is possible that the decrease in brightness temperature and increase in magnitude of updraft helicity in the warmer simulation is due to an increase in offshore CAPE. However, it is also possible that the increase in predicted storm severity is due to increases in shear.

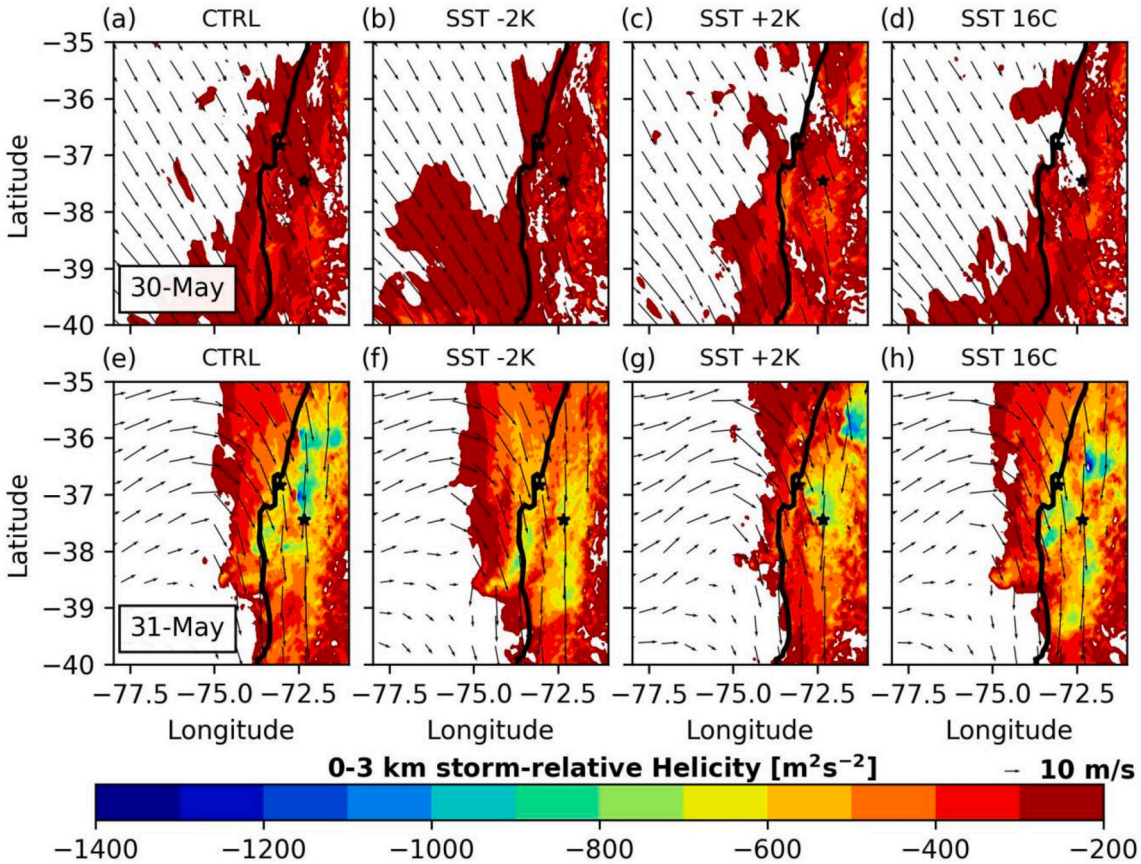

Fig. 16. The 0–3 km storm-relative helicity (in $m^2\,s^{-2}$) for (a) the CTRL, (b) SST-2 K, (c) SST + 2 K, and (d) SST16C simulations for 30 May 2019 at 2150 UTC (1750 LT), and the same in (e)-(h) except for 31 May 2019 at 1800 UTC (1400 LT). Wind vectors represent the wind field at 900 hPa. Black stars show the locations of the cities of Los Angeles and Concepción.

4.3. Combined effects of terrain and SST

To help resolve those differences, two additional sensitivity simulations were performed: SST-2 K_0p (colder SSTs with no topography) and SST + 2 K_0p (warmer SSTs with no topography). When SSTs were warmed and topography lowered, the 0–6-km bulk shear over the study region on both days was 6–12 $m\,s^{-1}$ (Figs. 17c,f), which was 10–12 $m\,s^{-1}$ lower than in the CTRL simulation (Figs. 17a,d) and in the simulation with full topography and warmer SSTs (SST + 2 K) (Figs. 15c,g). The simulation with colder SSTs and no topography (SST-2 K_0p) showed similar behavior in both days (Fig. 17b,e). Values of SRH were also reduced when topography was lowered and SST increased (not shown). These results indicate that topography, not SST, was the main factor that favored the high wind shear values present on both days.

Removing the topography caused CAPE values in both the colder (SST-2 K_0p) and warmer (SST + 2 K_0p) simulations to generally decrease over the ocean and to increase over land by 200–500 $J\,kg^{-1}$ (Figs. 18b,c,e,f), compared to both the CTRL simulation (Figs. 18a,d) and the corresponding simulations with the same SST changes but with full topography (Figs. 12b,c,f,g). The decrease in CAPE over the ocean in both simulations without topography (SST-2 K_0p and SST + 2 K_0p) negatively affected the area and intensity of the convection that developed both days. Fewer and less intense convective cells developed on 30 May and 31 May 2019 when topography was removed, resulting in just a few updraft helicity swaths in the region (Fig. 19). These final two simulations highlight the vital role the Andes topography plays, both in developing large values of wind shear and SRH on its western side and in enhancing CAPE values over the ocean. They also highlight the lesser, but not insignificant, role of SST anomalies in the near-coastal

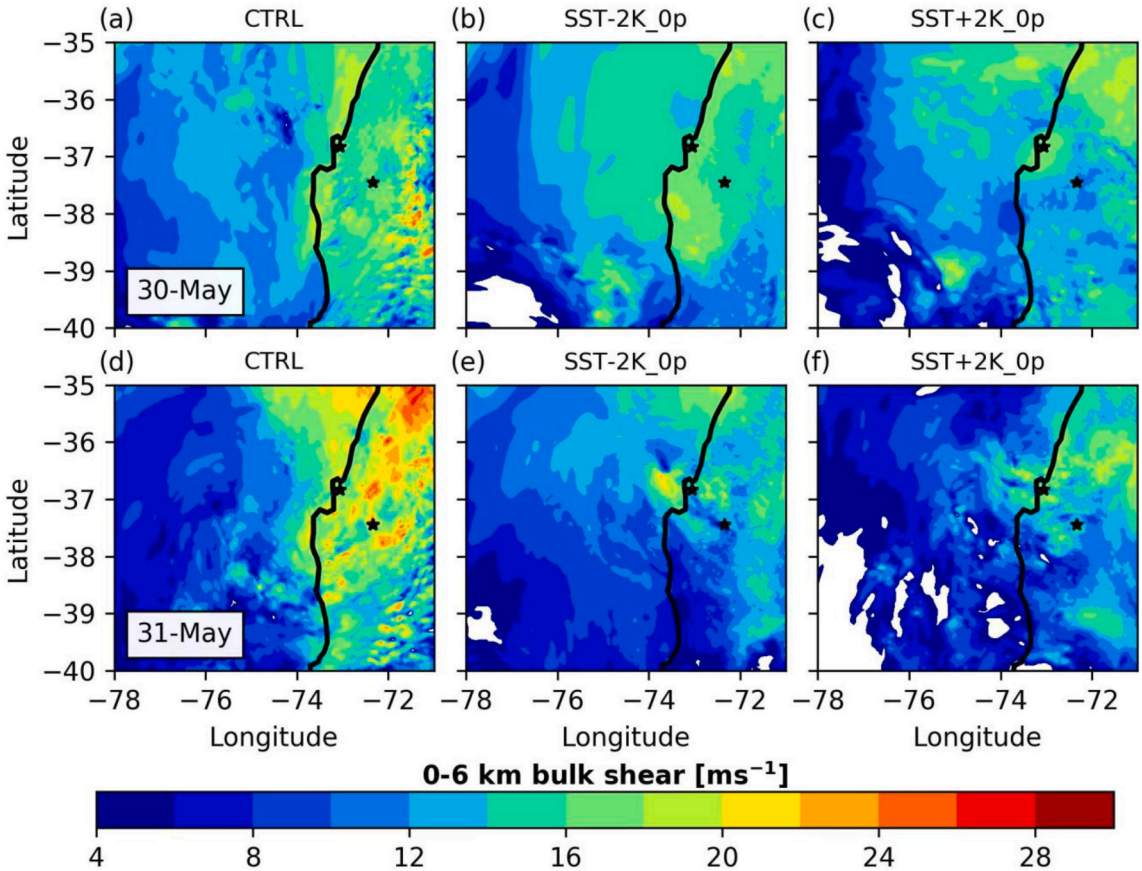

Fig. 17. The 0–6 km bulk shear (in m s^{-1}) for (a) the CTRL, (b) SST-2 K_0p, and (c) SST + 2 K_0p for 30 May 2019 at 2150 UTC (1750 LT), and the same in (d)-(f) except for 31 May 2019 at 1800 UTC (1400 LT). Black stars show the locations of the cities of Los Angeles and Concepción.

zone of south-central Chile, whereby warmer SSTs can aid storm severity and cooler SSTs can diminish it.

5. Conclusions and discussion

This study analyzed the impacts of the Andes mountains and the SST anomalies in providing the conditions favorable for tornadogenesis. To do so, a control and eight sensitivity simulations were conducted: three simulations whereby the topography was successively lowered to 0% of original; three simulations where SSTs were increased (by 2 K everywhere), decreased (by 2 K everywhere), and the SST gradient was relaxed (by setting all SSTs greater than 16 °C to 16 °C); and two simulations that combined SST increases and decreases with 0% topography. The sensitivity simulations to the terrain height showed the important role of the topography in the generation of favorable conditions for tornadogenesis. The southern Andes mountains helped intensify a northerly low- to mid-level jet flowing parallel to its western side as a result of flow-blocking. This jet was more intense on 31 May 2019 since the mid-level trough and surface cyclone were closer to the coast (see B20). This northerly barrier jet generated large values of 0–6-km bulk shear and 0–3-km SRH on both days that decreased when topography was reduced. The topography had a positive role in forming storms with mid-level (2–5-km) rotation (a condition very favorable for tornadogenesis), seen in updraft helicity swaths that decreased with decreasing topography.

The sensitivity of these environments to SSTs was also explored. When SSTs were increased by 2 K, offshore values of CAPE increased by 200–400 J kg^{-1}, and when SSTs were decreased by 2 K, offshore values of CAPE decreased by approximately the same amount. Values of CAPE over land were more complex, perhaps because the increase in SST led

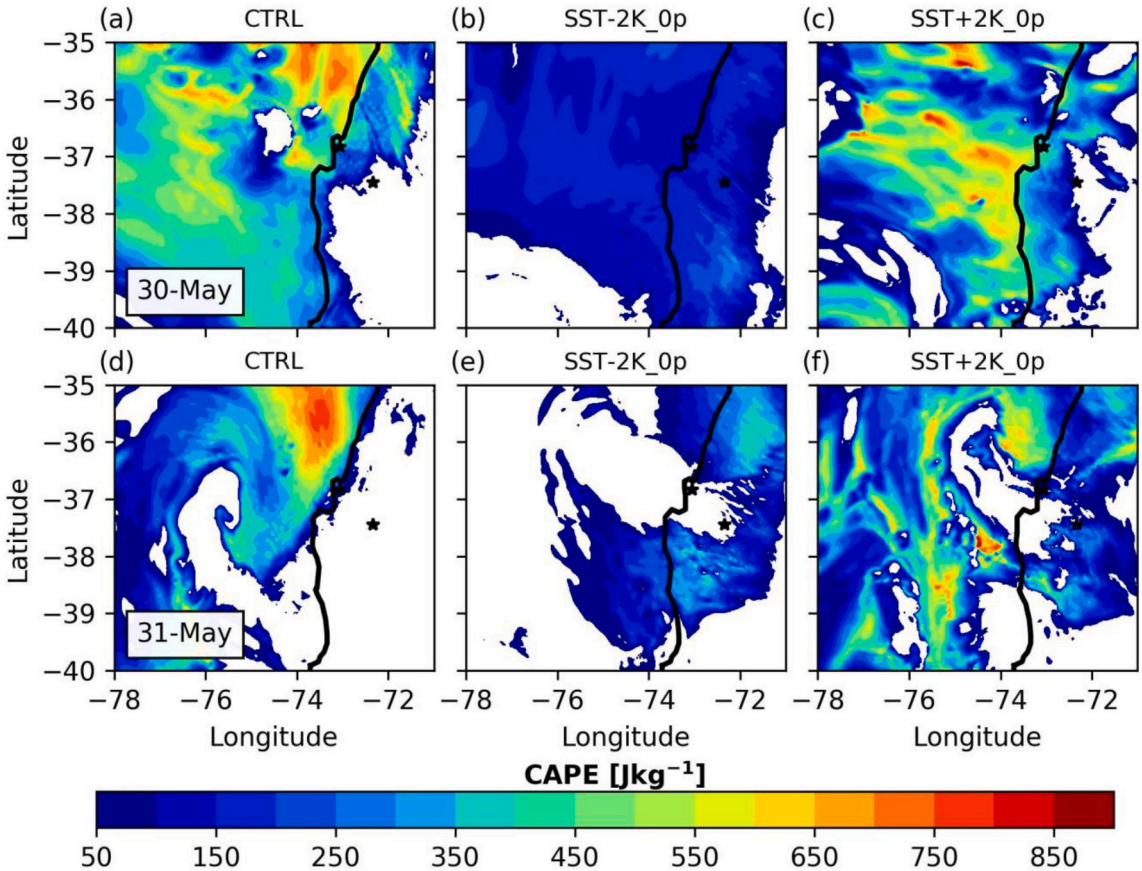

Fig. 18. Horizontal distribution of CAPE (in J kg^{-1}) for (a) the CTRL, (b) SST-2 K_0p, and (c) SST + 2 K_0p, for 30 May 2019 at 2150 UTC (1750 LT), and the same in (d)-(f) except for 31 May 2019 at 1800 UTC (1400 LT). Black stars show the locations of the cities of Los Angeles and Concepción.

to more widespread coverage of convection and thus decrease of inland CAPE. Because the tornadoes already formed in a low-CAPE, high-shear mesoscale environment, any increase in CAPE would be significant.

Finally, to explore which of the two factors (topography or SST) may have been most important to the tornado formation on 30 and 31 May 2019, sensitivity simulations were conducted that changed both at the same time. Helicity swaths confirmed that topography (and thus its accompanying increase in wind shear) seemed to be more important than SST at generating updraft rotation. This result suggests that shear is more important than CAPE for tornadic storms in Chile (similar to other regions in the world), and operational meteorologists concerned about possible tornado formation in Chile should pay very close attention to the synoptic- and mesoscale conditions (surface and upper-level cyclone; flow regimes that support blocking and low-level jet formation), and not discount those conditions even if SSTs are below normal.

Declaration of Competing Interest

The authors declare that they have no known competing financial interests or personal relationships that could have appeared to influence the work reported in this paper.

Acknowledgments

This work was supported by Conicyt [grant number MEC80180038] and the U.S. National Science Foundation [grant number OPP 1821915]. JCM and DP acknowledge financial support from Centro de Estudios Atmosféricos y Astroestadística (CEAAS), Universidad de Valparaíso. Powered@NLHPC: This research was partially supported by the supercomputing infrastructure of the National Laboratory for High Performance Computing (ECM-02). the award from the U.S. National Science Foundation [grant number OPP 1821915].

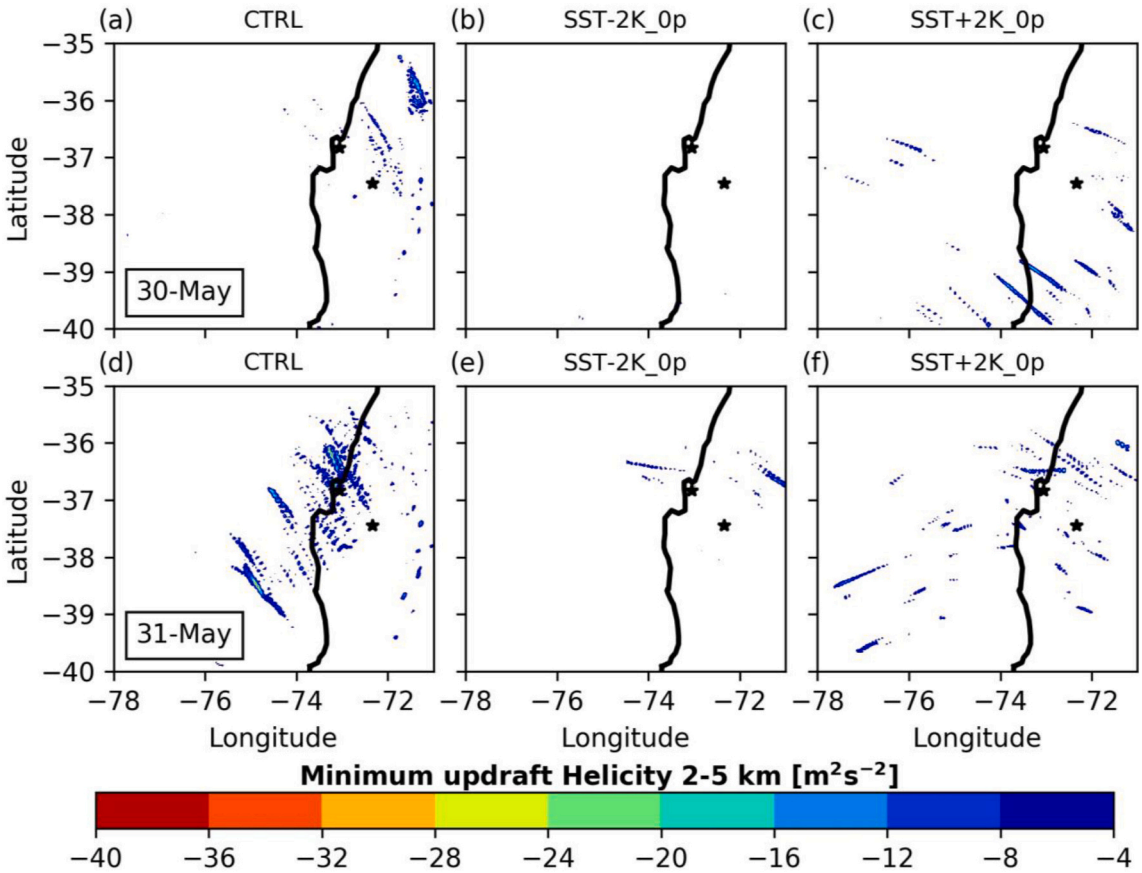

Fig. 19. Minimum model updraft helicity in the 2–5-km layer (color shaded; $m^2\ s^{-2}$) for (a) the CTRL, (b) SST-2 K_0p, and (c) SST + 2 K_0p, for 1950–2350 UTC (1550–2150 LT) 30 May 2019, and the same in (d)-(f) except for 1600–2000 UTC (1200–1600 LT) 31 May 2019. Black stars show the locations of the cities of Los Angeles and Concepción.

References

Aceituno, P., 1993. Climate along the extratropical west coast of South America. In: Earth System Responses to Global Change: Contrasts between North and South America. 61-69. pp. 1993.

Aguirre, C., Rojas, M., Garreaud, R.D., Rahn, D.A., 2019. Role of synoptic activity on projected changes in upwelling-favourable winds at the ocean's eastern boundaries. Clim. Atmos. Sci. 2, 44. https://doi.org/10.1038/s41612-019-0101-9.

Barrett, B.S., Marín, J.C., Jacques-Coper, M., 2020. A multiscale analysis of the tornadoes of 30-31 May 2019 in south-Central Chile. Atmos. Res. 236, 104811. https://doi.org/10.1016/j.atmosres.2019.104811.

Barrett, B.S., Gensini, V.A., 2013. Variability of Central United States April–May tornado day likelihood by phase of the Madden-Julian Oscillation. Geophys. Res. Lett. 40, 2790–2795.

Barrett, B.S., Hameed, S., 2017. Seasonal variability in precipitation in Central and Southern Chile: modulation by the South Pacific High. J. Climate 30, 55–69.

Barrett, B.S., Garreaud, R., Falvey, M., 2009. Effect of the Andes Cordillera on precipitation from a midlatitude cold front. Mon. Weather Rev. 137, 3092–3109. https://doi.org/10.1175/2009MWR2881.1.

Barrett, B.S., Krieger, D.B., Barlow, C.P., 2011. Multiday circulation and precipitation climatology during winter rain events of differing intensities in Central Chile. J. Hydrometeorol. 12, 1071–1085. https://doi.org/10.1175/2011JHM1377.1.

Barrett, B.S., Campos, D., Vicencio, J., Rondanelli, R., 2016. Extreme temperature and precipitation events in March 2015 in central and northern Chile. J. Geophys. Res. Atmos. 121, 4563–4580. https://doi.org/10.1002/2016JD024835.

Blier, W., Batten, K.A., 1994. On the incidence of tornadoes in California. Wea. Forecast. 9, 301–315.

Bozkurt, D., Rondanelli, R., Garreaud, R., Arriagada, A., 2016. Impact of warmer eastern tropical Pacific SST on the March 2015 Atacama floods. Mon. Weather Rev. 144 (11), 4441–4460.

Brooks, H.E., Lee, J.W., Craven, J.P., 2003. The spatial distribution of severe thunderstorm and tornado environments from global reanalysis data. Atmos. Res. 67–68, 73–94.

Brooks, H.E., Doswell III, C.A., Zhang, X., Chernokulsky, A., Tochimoto, E., Hanstrum, B., Nascimento, E., Sills, D.M.L., Antonescu, B., Barrett, B.S., 2019. A century of progress in severe convective storm research and forecasting. Meteorol. Monogr. 59, 18.1–18.41. https://doi.org/10.1175/AMSMONOGRAPHS-D-18-0026.1.

Bunkers, M.J., Klimowski, B.A., Zeitler, J.W., Thompson, R.L., Weisman, M.L., 2000. Predicting supercell motion using a new hodograph technique. Wea. Forecast. 15, 61–79.

Chen, T.C., Kpaeyeh, J.A., 1993. The synoptic-scale environment associated with the low-level jet of the Great Plains. Mon. Weather Rev. 121, 416–420.

Chen, S., Lin, Y., 2005. Effects of moist Froude number and CAPE on a conditionally unstable flow over a mesoscale mountain ridge. J. Atmos. Sci. 62, 331–350. https://doi.org/10.1175/JAS-3380.1.

Clark, M.R., 2009. The southern England tornadoes of 30 december 2006: Case study of a tornadic storm in a low CAPE, high shear environment. Atmos. Environ. 93, 50–65. https://doi.org/10.1016/j.atmosres.2008.10.008.

Clark, A.J., Gao, J., Marsh, P.T., Smith, T., Kain, J.S., Correia, J., Xue, M., Kong, F., 2013. Tornado pathlength forecasts from 2010 to 2011 using ensemble updraft helicity. Wea. Forecast. 28, 387–407. https://doi.org/10.1175/WAF-D-12-00038.1.

Cohen, A.E., 2010. Indices of violent tornado environments. Electron. J. Oper. Meteor. 11 2010-EJ6. Available online at. http://www.nwas.org/ej/pdf/2010-EJ6.pdf.

Davies-Jones, R.P., 1986. Tornado dynamics. In: Kessler, E. (Ed.), Thunderstorm Morphology and Dynamics. University of Oklahoma Press, Norman, pp. 197–236.

Davies-Jones, R.P., Burgess, D.W., Foster, M., 1990. Test of helicity as a tornado forecast parameter. Preprints. In: 16th Conf. On Severe Local Storms, Kananaskis Park, AB, Canada, pp. 588–592 Amer. Meteor. Soc.

Doswell III, C.A., Brooks, H.E., Maddox, R.A., 1996. Flash-flood forecasting: an ingredients-based methodology. Weather Forecast. 11, 360–381.

Emanuel, K.A., 1994. Atmospheric Convection. Oxford University Press 580 pp.

Garreaud, R., 2009. The Andes climate and weather. Adv. Geosci. 7, 1–9.

Garreaud, R., Muñoz, R.C., 2005. The low-level jet off the west coast of subtropical South America: Structure and variability. Mon. Weather Rev. 133, 2246–2261. https://journals.ametsoc.org/mwr/article/133/8/2246/67555.

Grünwald, S., Brooks, H.E., 2011. Relationship between sounding derived parameters and the strength of tornadoes in Europe and the USA from reanalysis data. Atmos. Res. 100, 479–488. https://doi.org/10.1016/j.atmosres.2010.11.011.

Hanstrum, B.N., Mills, G.A., Watson, A., 1998. Australian cool season tornadoes. Part 1: Synoptic climatology. In: Preprints, 19th Conf. On Severe Local Storms. Amer. Meteor. Soc., Minneapolis, MN, Pp. 97–100.

Hanstrum, B.N., Mills, G.A., Watson, A., Monteverdi, J.P., Doswell, C.A., 2002. The cool-season tornadoes of California and southern Australia. Wea. Forecast. 17, 705–722. https://doi.org/10.1175/1520-0434(2002).

Houston, A.L., Thompson, R.L., Edwards, R., 2008. The Optimal Bulk Wind Differential Depth and the Utility of the Upper-Tropospheric Storm-Relative Flow for forecasting Supercells. Wea. Forecast. 23, 825–837. https://doi.org/10.1175/

2008WAF2007007.1.
Iacono, M.J., Delamere, J.S., Mlawer, E.J., Shephard, M.W., Clough, S.A., Collins, W.D., 2008. Radiative forcing by long–lived greenhouse gases: Calculations with the AER radiative transfer models. J. Geophys. Res. 113, D13103. https://doi.org/10.1029/2008JD009944.
Janjic, Z.I., 1994. The step–mountain eta coordinate model: further developments of the convection, viscous sublayer, and turbulence closure schemes. Mon. Weather Rev. 122, 927–945.
Kounkou, R., Mills, G., Timbal, B., 2009. A reanalysis climatology of cool-season tornado environments over southern Australia. Int. J. Climatol. 29, 2079–2090. https://doi.org/10.1002/joc.1856.
LaPenta, K.D., Bosart, L.F., Galarneau, T.J., Dickinson, M.J., 2005. A multiscale examination of the 31 May 1998 Mechanicsville, New York, tornado. Wea. Forecast. 20, 494–516.
Markowski, P.M., Richardson, Y.P., 2009. Tornadogenesis: our current understanding, forecasting considerations, and questions to guide future research. Atmos. Res. 93, 3–10.
Markowski, P., Richardson, Y., 2014. What we know and don't know about tornado formation. Phys. Today 67, 26–31.
Markowski, P.M., Straka, J.M., 2000. Some observations of rotating updrafts in a low-buoyancy, highly sheared environment. Mon. Weather Rev. 128, 449–461. https://doi.org/10.1175/1520-0493(2000)128<0449:SOORUI>2.0.CO;2.
Marwitz, J.D., 1987. Deep orographic storms over the Sierra Nevada. Part I: thermodynamic and kinematic structure. J. Atmos. Sci. 44, 159–173.
Matsangouras, I.T., Pytharoulis, I., Nastos, P.T., 2014. Numerical modeling and analysis of the effect of complex Greek topography on tornadogenesis. Nat. Hazards Earth Syst. Sci. 14, 1905–1919. https://doi.org/10.5194/nhess-14-1905-2014.
Matsangouras, I., Nastos, P., Pytharoulis, I., 2016. Study of the tornado event in Greece on March 25, 2009: Synoptic analysis and numerical modeling using modified topography. Atmos. Res. 169, 566–583.
Miglietta, M.M., Mazon, J., Rotunno, R., 2017. Numerical simulations of a tornadic supercell over the Mediterranean. Wea. Forecast. 32, 1209–1226. https://doi.org/10.1175/WAF-D-16-0223.1.
Molina, M.J., Allen, J.T., 2019. On the moisture origins of tornadic thunderstorms. J. Clim. 32, 4321–4346. https://doi.org/10.1175/JCLI-D-18-0784.1.
Molina, M.J., Timmer, R.P., Allen, J.T., 2016. Importance of the Gulf of Mexico as a climate driver for U.S. severe thunderstorm activity. Geophys. Res. Lett. 43, 12 295–12 304. https://doi.org/10.1002/2016GL071603.
Molina, M.J., Allen, J.T., Gensini, V.A., 2018. The Gulf of Mexico and ENSO influence on subseasonal and seasonal CONUS winter tornado variability. J. Appl. Meteor. Climatol. 57, 2439–2463. https://doi.org/10.1175/JAMC-D-18-0046.1.
Montecinos, A., Aceituno, P., 2003. Seasonality of the ENSO-related rainfall variability in Central Chile and associated circulation anomalies. J. Clim. 16, 281–296.
Monteverdi, J.P., Quadros, J., 1994. Convective and rotational parameters associated with three tornado episodes in northern and Central California. Wea. Forecast. 9, 285–300.
Muñoz, R.C., Garreaud, R., 2005. Dynamics of the low-level jet off the west coast of subtropical South America. Mon. Weather Rev. 133 (12), 3661–3677. https://journals.ametsoc.org/mwr/article/133/12/3661/67511.
Nakanishi, M., Niino, H., 2006. An improved Mellor–Yamada level 3 model: its numerical stability and application to a regional prediction of advecting fog. Bound. Layer Meteor. 119, 397–407. https://doi.org/10.1007/s10546-005-9030-8.
Niu, G.-Y., Yang, Z.-L., Mitchell, K.E., Chen, F., Ek, M.B., Barlage, M., Kumar, A., Manning, K., Niyogi, D., Rosero, E., Tewari, M., Xia, Y., 2011. The community Noah land surface model with multiparameterization options (Noah–MP): 1. Model description and evaluation with local–scale measurements. J. Geophys. Res. 116, D12109. https://doi.org/10.1029/2010JD015139.
Overland, J.E., Bond, N.A., 1993. The influence of coastal orography: the Yakutat storm. Mon. Weather Rev. 121, 1388–1397.
Parish, T.R., 1982. Barrier winds along the Sierra Nevada mountains. J. Appl. Meteorol. 21, 925–930.
Potvin, C.K., Elmore, K.L., Weiss, S.J., 2010. Assessing the impacts of proximity sounding criteria on the climatology of significant tornado environments. Wea. Forecast. 25, 921–930. https://doi.org/10.1175/2010WAF2222368.1.
Rasmussen, E.N., 2003. Refined supercell and tornado forecast parameters. Wea. Forecast. 18, 530–535. https://doi.org/10.1175/1520-0434(2003)18<530:RSATFP>2.0.CO;2.
Rasmussen, E.N., Blanchard, D.O., 1998. A baseline climatology of sounding-derived supercell and tornado forecast parameters. Wea. Forecast. 13, 1148–1164.
Rutllant, J., Fuenzalida, H., 1991. Synoptic aspects of the Central Chile rainfall variability associated with the Southern Oscillation. Int. Journal of Clim. 11, 63–76.
Sherburn, K.D., Parker, M.D., 2014. Climatology and ingredients of significant severe convection in high-shear, low-CAPE environments. Wea. Forecasting. 29, 854–877. https://doi.org/10.1175/WAF-D-13-00041.1.
Sherburn, K.D., Parker, M.D., King, J.R., Lackmann, G.M., 2016. Composite environments of severe and nonsevere high-shear, low-CAPE convective events. Wea. Forecast. 31, 1899–1927. https://doi.org/10.1175/WAF-D-16-0086.1.
Skamarock, W.C., Klemp, J.B., Dudhia, J., Gill, D.O., Liu, Z., Berner, J., Wang, W., Powers, J.G., Duda, M.G., Barker, D.M., Huang, X.Y., 2019. A Description of the Advanced Research WRF Model Version 4 (No. NCAR/TN-556+ STR). National Center for Atmospheric Research. 145 pp. Boulder, CO, USA.
Tang, B., Vaughan, M., Lazear, R., Corbosiero, K., Bosart, L., Wasula, T., Lee, I., Lipton, K., 2016. Topographic and boundary influences on the 22 May 2014 Duanesburg, New York, tornadic supercell. Wea. Forecast. 31, 107–127.
Thompson, R.L., Edwards, R., Hart, J.A., Elmore, K.L., Markowski, P., 2003. Close proximity soundings within supercell environments obtained from the rapid update cycle. Wea. Forecast. 18, 1243–1261.
Thompson, R.L., Edwards, R., Mead, C.M., 2004. An update to the supercell composite and significant tornado parameters. Preprints. 22nd Conf. Severe Local Storms, Hyannis, MA, Amer. Meteor. Soc P8.1. Available online at. https://ams.confex.com/ams/pdfpapers/82100.pdf.
Thompson, R.L., Mead, C.M., Edwards, R., 2007. Effective storm-relative helicity and bulk shear in supercell thunderstorm environments. Wea. Forecast. 22, 102–115. https://doi.org/10.1175/WAF969.1.
Thompson, G., Field, P.R., Rasmussen, R.M., Hall, W.D., 2008. Explicit forecasts of winter precipitation using an improved bulk microphysics scheme. Part II: implementation of a new snow parameterization. Mon. Wea. Rev. 136, 5095–5115. https://doi.org/10.1175/2008MWR2387.1.
Viale, M., Garreaud, R., 2015. Orographic effects of the subtropical and extratropical Andes on upwind precipitating clouds. J. Geophys. Res. Atmos. 120. https://doi.org/10.1002/2014JD023014.
Viale, M., Norte, F.A., 2009. Strong cross-barrier flow under stable conditions producing intense winter orographic precipitation: a case study over the subtropical Central Andes. Wea. Forecast. 24, 1009–1031. https://doi.org/10.1175/2009WAF2222168.1.
Viale, M., Nuñez, M.N., 2011. Climatology of winter orographic precipitation over the subtropical Central Andes and associated synoptic and regional characteristics. J. Hydrometeorol. 12, 481–507. https://doi.org/10.1175/2010JHM1284.1.
Viale, M., Houze, R.A., Rasmussen, K.L., 2013. Upstream Orographic Enhancement of a Narrow Cold-Frontal Rainband Approaching the Andes. Mon. Weather Rev. 141, 1708–1730. https://doi.org/10.1175/MWR-D-12-00138.1.
Vicencio, J., Reyes, A., Sánches, S., Padilla, R., Crespo, J., Campos, D., 2019. Informe especial: Tornados en la Región del Biobío. pp. 40. http://archivos.meteochile.gob.cl/portaldmc/meteochile/documentos/DMC-InfoEspecial_TornadosBiobio_v5black.pdf.
Wesolek, E., Mahieu, P., 2011. The F4 tornado of August 3, 2008, in Northern France: case study of a tornadic storm in a low CAPE environment. Atmos. Res. 100, 649–656. https://doi.org/10.1016/j.atmosres.2010.09.003.
Yu, C.-K., Smull, B.F., 2000. Airborne Doppler observations of a landfalling cold front upstream of steep coastal orography. Mon. Weather Rev. 128, 1577–1603.